

Article

Benzimidazole-Based NHC Metal Complexes as Anticancer Drug Candidates: Gold(I) vs. Platinum(II)

Paul Kapitza ¹, Patricia Grabher ¹, Amelie Scherfler ¹, Klaus Wurst ², Brigitte Kircher ³, Ronald Gust ¹ and Hristo P. Varbanov ^{1,4,*}

¹ Department of Pharmaceutical Chemistry, Institute of Pharmacy, University of Innsbruck, Innrain 80/82, 6020 Innsbruck, Austria; paul.kapitza@uibk.ac.at (P.K.)

² Department of General, Inorganic and Theoretical Chemistry, University of Innsbruck, Innrain 80/82, 6020 Innsbruck, Austria

³ Department of Internal Medicine V (Hematology and Oncology), Medical University Innsbruck, Anichstraße 35, 6020 Innsbruck, Austria

⁴ Medical College, Trakia University—Stara Zagora, 9 Armeiska str., 6003 Stara Zagora, Bulgaria

* Correspondence: hristo.varbanov@uibk.ac.at

Abstract: Herein, we present a comparative study on the chemistry and biological activity of *N*-heterocyclic carbene (NHC)Pt(II)/Au(I) complexes. Accordingly, representative compounds of the *cis/trans*- [PtL₂X₂] (X = Cl (5, 6) or I (7, 8)), [PtL₃Cl]⁺ (9), [AuLX] (X = Cl (10) or I (11)), and [AuL₂]⁺ (12) type, where L is 1,3-diethylbenzimidazol-2-ylidene, were synthesized and characterized in detail to elucidate the role of the metal center on their physicochemical and biological properties. The stability of the complexes in the presence of cell culture medium and their reactivity toward relevant biomolecules were investigated by RP-HPLC. In addition, their effects on plasmid DNA and *in vitro* cytotoxicity in ovarian cancer cells and non-malignant fibroblasts were evaluated. Cationic [AuL₂]⁺ and [PtL₃X]⁺ species displayed the highest cytotoxicity and stability in cell culture medium in the series. They exhibited IC₅₀ values lower than the established metallodrugs cisplatin and auranofin in both wild-type and cisplatin-resistant ovarian cancer cells, being able to circumvent cisplatin resistance. Finally, Pt(II)–NHC complexes form 5'-guanosine monophosphate adducts under physiologically relevant conditions and interact with plasmid DNA in contrast to their Au(I) analogs, corroborating their distinct modes of action.

Keywords: NHC; platinum(II); gold(I); crystal structures; ovarian cancer; A2780; DNA



check for updates

Citation: Kapitza, P.; Grabher, P.; Scherfler, A.; Wurst, K.; Kircher, B.; Gust, R.; Varbanov, H.P. Benzimidazole-Based NHC Metal Complexes as Anticancer Drug Candidates: Gold(I) vs. Platinum(II). *Inorganics* **2023**, *11*, 293. <https://doi.org/10.3390/inorganics11070293>

Academic Editor: Antonio Laguna

Received: 16 June 2023

Revised: 6 July 2023

Accepted: 7 July 2023

Published: 11 July 2023



Copyright: © 2023 by the authors. Licensee MDPI, Basel, Switzerland. This article is an open access article distributed under the terms and conditions of the Creative Commons Attribution (CC BY) license (<https://creativecommons.org/licenses/by/4.0/>).

1. Introduction

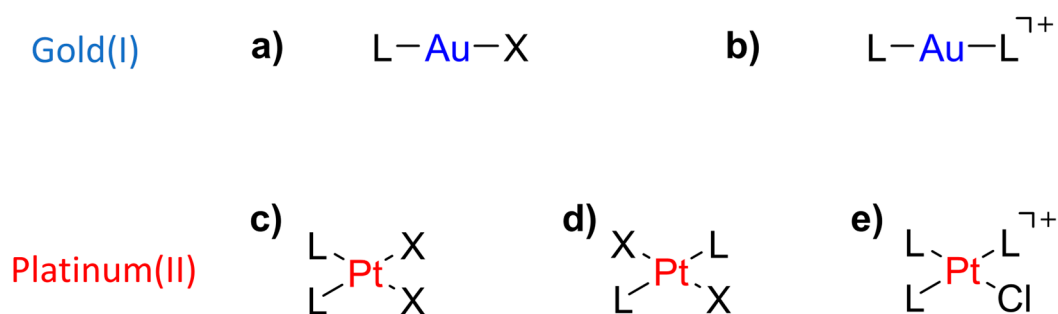
Over 50 years after the discovery of the antiproliferative effects of cisplatin [1], platinum-based chemotherapeutics remain among the most extensively used drugs in oncology [2,3]. Nevertheless, their clinical effectiveness is limited due to severe side effects and resistance phenomena [4–10]. To address these shortcomings, numerous bioactive metal complexes have been developed during the last decades and their potential application as anticancer agents has been evaluated [5,11–17]. In the search for new organic ligands for the development of catalysts and metallodrugs, the use of *N*-heterocyclic carbenes (NHC) emerged in 1991 with the isolation of the first free carbene [18]. This relatively new class of ligands stabilizes the metal center by forming strong metal–carbon bonds due to their σ -donor and π -backbonding properties [19,20]. Accordingly, stable and structurally diverse metal–NHC complexes can be obtained by relatively straightforward synthetic procedures [21–24]. In addition to their ability to catalyze numerous reactions [25,26], a good number of NHC compounds are used as stabilizing agents for nanoparticles and clusters [27,28]. Furthermore, some metal NHC complexes showed to be promising candidates as new chemotherapeutics to overcome the limitations of current clinically used platinum

drugs. In particular, gold and platinum NHC complexes have demonstrated considerable activity against various chemo-resistant bacteria and cancer cells [29–34].

The generally accepted mechanism of action of platinum(II) drugs involves covalent binding to the DNA with the formation of DNA adducts [10]. Several studies have demonstrated that Pt(II)–NHC complexes also interact with DNA, although in a different way than cisplatin and its analogs [35,36]. In some cases, electrostatic interactions with DNA proved to be of higher relevance for the cytotoxicity of Pt(II/IV)–NHC complexes than covalent binding to DNA [32]. The main potential molecular targets considered for the Au(I)–NHC complexes include the selenoenzymes glutathione peroxidase (GPx) [37,38] and, particularly, the thioredoxin reductase (TrxR) [38–42].

Complexes of the type [Au(NHC)X] (X = Cl, Br, I) are readily transformed in aqueous media to cationic [Au(NHC)₂]⁺ species due to an effect called ligand scrambling [39,43–45]. This type of compounds showed remarkably high cytotoxic effects in numerous cancer cell lines and a higher cellular accumulation, and thus may contribute to the activity of [Au(NHC)X] complexes as their more active metabolites. To date, the exact intracellular target of [Au(NHC)₂]⁺ complexes has not been identified beyond doubt. Their interaction with the classical targets of the halido Au(I)–NHC complexes—namely, GPx or TrxR—is questionable due to their high stability toward nucleophiles (e.g., thiols such as cysteine) [39]. Moreover, the strong antiproliferative activity of [Au(NHC)₂]⁺ complexes does not correlate with their inhibitory effect on TrxR [38,39]. Another possible target would be G-quadruplex-DNA, as postulated by Casini et al. [46,47].

Despite the numerous publications on cytotoxic Au(I)– and Pt(II)–NHC complexes [16,32,35,36,48–50], no comparative investigation of their physicochemical and biological properties has been reported so far. In this work, we intend to fill this gap and elucidate the effect of the metal center (Pt(II) vs. Au(I)) on the chemistry (synthesis, solubility, stability) and pharmacological profile (cytotoxicity, interaction with biomolecules) of NHC complexes. Accordingly, the already known NHC complexes of the type [AuLX] (X = Cl or I) and [AuL₂]⁺, where L is 1,3-diethylbenzimidazol-2-ylidene, and the corresponding new platinum(II) species (see Scheme 1) have been synthesized and structurally characterized. Their cytotoxicity was examined in the ovarian carcinoma cell lines A2780wt and A2780cis (cisplatin-resistant subvariant) as well as in non-malignant fibroblast cells. To obtain further insights into the mechanism of action of the complexes, their effect on plasmid DNA and potential interactions with representative biomolecules was also investigated.

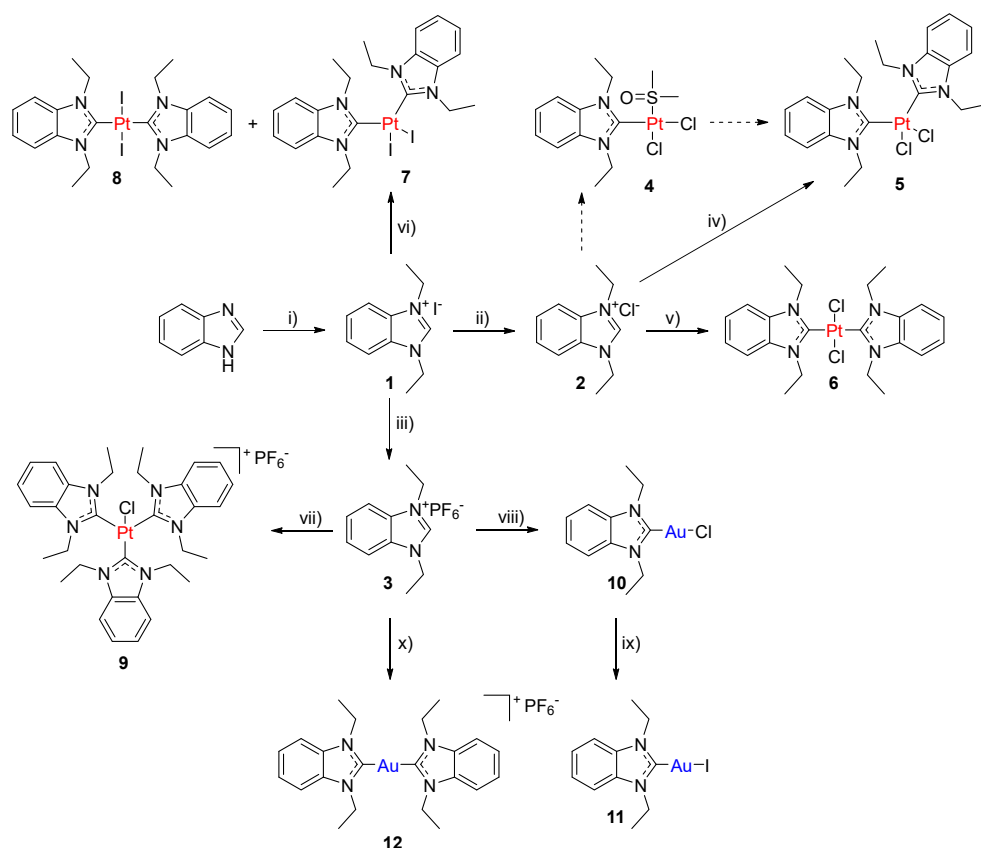


Scheme 1. Au(I)– and Pt(II)–NHC complexes under investigation: **a)** [AuLX], **b)** [AuL₂]⁺, **c)** *cis*-[PtL₂X₂], **d)** *trans*-[PtL₂X₂], **e)** [PtL₃Cl]⁺; L = 1,3-diethylbenzimidazol-2-ylidene, X = Cl, I.

2. Results

2.1. Synthesis and Characterisation

The synthesis of complexes 5–12 was performed in a multistep procedure as depicted in Scheme 2.



Scheme 2. Synthetic routes to obtain complexes 5–12. **i)** NaH, EtI, ACN, 82 °C; **ii)** Ag₂SO₄, BaCl₂, H₂O, rt; **iii)** KPF₆, MeOH/H₂O, rt; **iv)** NaOMe, *cis*-[Pt(DMSO)₂Cl₂], ACN, rt; **v)** Ag₂O, K₂[PtCl₄], DCM, rt; **vi)** NaOtBu, *cis*-[Pt(DMSO)₂I₂], DCM, rt; **vii)** KPF₆, NaOtBu, *cis*-[Pt(DMSO)₂Cl₂], DCM, 40 °C (method A) or KPF₆, NaOMe, *cis*-[Pt(DMSO)LCI₂], DCM, 30 °C (method B); **viii)** Ag₂O, LiCl, [Au(SMe)₂Cl], DCM/MeOH, rt; **ix)** NaI, acetone, rt; **x)** Ag₂O, [Au(SMe)₂Cl], DCM/MeOH, rt.

Gold(I) complexes 10–12 [51] were prepared starting from 1,3-diethylbenzimidazol-2-ium hexafluorophosphate following established protocols [39] (see also Section 3).

In contrast to gold(I), which only allows the coordination of two ligands in a linear arrangement, platinum(II) complexes possess a square-planar geometry with a ligand sphere that can be occupied by four monodentate ligands. Accordingly, two isomeric forms (*cis* and *trans*) are possible for compounds of the [PtL₂X₂] type. The *trans*-[PtL₂Cl₂] complex 6 was prepared by performing a reaction of the silver carbene complex of ligand 2 (obtained in situ with Ag₂O) with K₂[PtCl₄] in DCM as previously described for similar compounds [52]. The corresponding *cis* isomer 5 could be synthesized from *cis*-[Pt(DMSO)LCI₂] (4) after reaction with the NHC ligand in the presence of a base [52] or directly from *cis*-[Pt(DMSO)₂Cl₂]. If *cis*-[Pt(DMSO)₂Cl₂] reacts with ligand 2 and NaOtBu (or NaOMe) as a base in anhydrous DCM, a mixture of the mono- and bis(carbene) complexes 4 and 5 is formed, where the amount of 5 depends on the equivalents (equiv.) of ligand used. Performing the reaction in ACN instead of DCM facilitated the isolation of complex 5, which precipitated from the reaction mixture due to its poor solubility. Interestingly, the reaction between *cis*-[Pt(DMSO)₂Cl₂], the hexafluorophosphate salt 3, and NaOtBu in anhydrous DCM resulted in a mixture of complex 5 and its tris(carbene) derivative 9. The latter could also be obtained by the reaction of 4 or 5 with ligand 3 in the presence of NaOMe. Purification by column chromatography and recrystallization(s) from MeOH allowed the isolation of 9 with sufficient purity (>95%).

Finally, the reaction between *cis*-[Pt(DMSO)₂I₂], ligand 1, and NaOtBu in anhydrous DCM resulted in a mixture of the *cis* and *trans* iodido complexes 7 and 8, which could be successfully separated and purified by column chromatography.

The synthesized Au(I)- and Pt(II)-NHC complexes were characterized in detail by multinuclear NMR spectroscopy, ESI-HRMS, Fourier-transform (FT)-IR spectroscopy, and X-ray crystallography (complexes **5**, **6**, **8**, **9**, **10**, **12**). The purity of all biologically tested compounds was verified by using RP-HPLC (>95%, see Figures S1–S7).

The disappearance of the carbene proton (N=CH-N) signal in the ^1H NMR spectra (Figures S8–S17) and the strong downfield shift of the signal for the carbon atom coordinated to the metal center in the ^{13}C NMR spectra (Figures S18–S25) are distinctive for the complex formation. The latter also allows discrimination of the complexes depending on the metal center, bound halide, and geometry (see Figure 1).

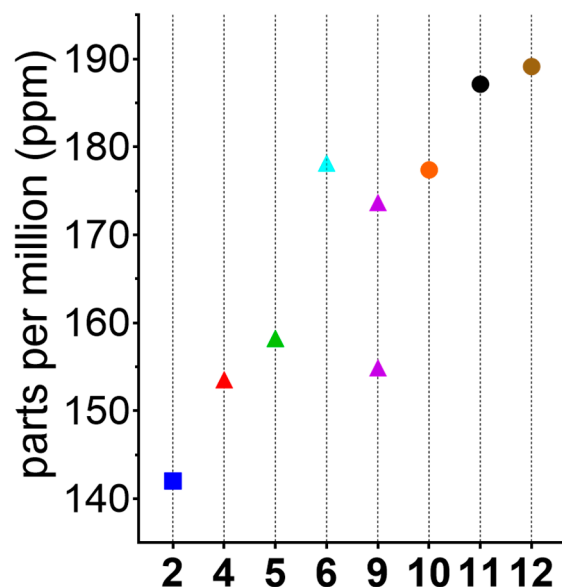


Figure 1. ^{13}C -Carbene signals of ligand **2** (■), platinum complexes **4–6** and **9** (▲), and gold complexes **10–12** (●) in CDCl_3 . The respective chemical shifts for complexes **7** and **8** could not be obtained due to insufficient solubility of the compounds.

In the case of the *cis*-configured compounds **5** and **7**, the N-CH₂ protons became chemically and magnetically different and split into separated signals with a multiplicity of a doublet from a quartet in the ^1H NMR spectra (Figures S10 and S12).

In contrast, the ^1H NMR spectra of the corresponding *trans* isomers **6** and **8** (Figures S11 and S13) showed the expected splitting of the methylene group into a quartet due to the neighboring of the methyl group. Since the *cis*- and the *trans*-configurations of **5** and **6/8** were confirmed via X-ray crystallography (vide infra), this finding can be used for the assignment of the complex's configuration. A comparable splitting was already described by Schobert et al. for related complexes [52]. It is worth mentioning that ^1H NMR spectra of the linear gold complexes (**10–12**) (Figures S15–S17) showed resonances of the N-CH₂-CH₃ protons comparable to the *trans*-configured platinum complexes **6/8**.

The cationic tris(carbene) platinum complex **9** displayed more complicated ^1H and ^{13}C NMR spectra with a double set of signals for the coordinated NHC ligands in a 1:2 ratio, and a splitting nearly identical to that of **5** and **6** in the ^1H NMR spectra (Figure S14). Two NHC ligands showed signals comparable to that of the *cis*-isomer **5**, while that of the third one was comparable to that of **6**. Clear differentiation between chlorido platinum complexes **5**, **6**, and **9** was also observed in the ^{195}Pt NMR with the tris(carbene) compound **9** exhibiting the most upfield shifted signal (see Figure S26). Finally, their identity was unambiguously confirmed by ESI-HRMS (see Figure S27) and X-ray crystallography (vide infra).

2.2. Crystal Structures

The molecular structures of ligand **1** and complexes **5**, **6**, **8–10**, and **12** were determined by single crystal X-ray diffraction analysis (see Figures 2, 3 and S28–S30). Suitable single crystals were obtained by slow evaporation of MeOH/CHCl₃ solutions of the respective compound. Selected bond lengths and angles are listed in Table 1.

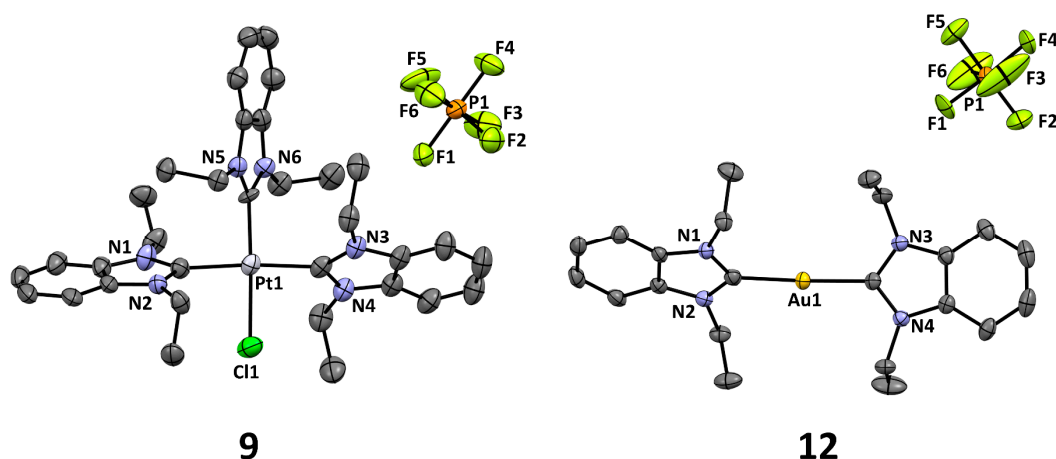


Figure 2. Molecular structures of cationic complexes **9** and **12**. For better visualization, solvent molecules and H atoms are not displayed. The thermal ellipsoids have been drawn at the 50% probability level.

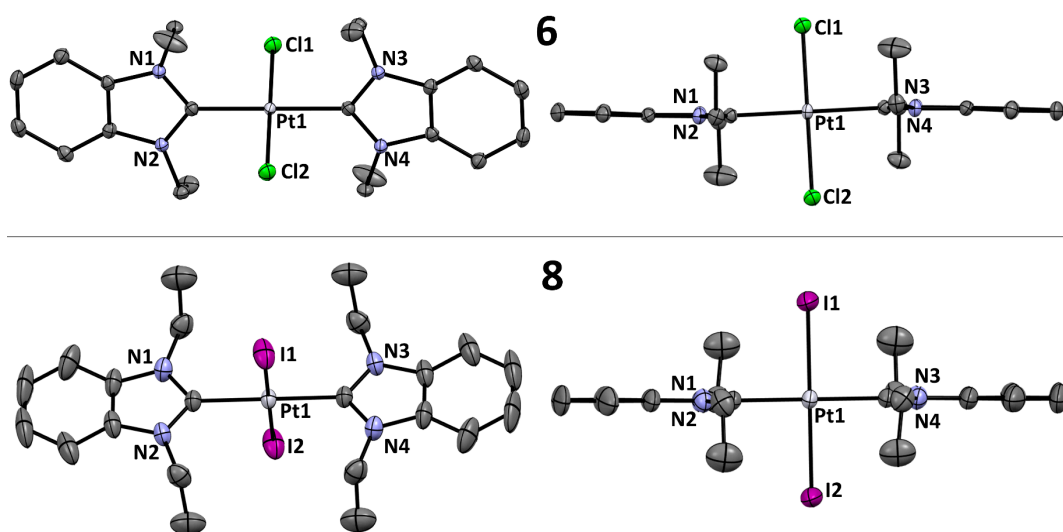


Figure 3. Molecular structures of complexes **6** and **8**. The thermal ellipsoids have been drawn at the 50% probability level (H atoms are omitted for clarity).

Crystal data and structure refinement details are provided in the Supplementary Materials (Tables S1–S7). The crystal structures of compounds **10** [51] and **12** [53] have already been reported. For the purpose of better comparability (same solvent composition for crystallization), the structures of these complexes were analyzed again in this study.

The metal–carbon bond lengths (1.975–2.041 Å) were nearly the same in all complexes. Interestingly, the M–X (M = Au or Pt, X = Cl or I) distance (2.275 Å (**10**), 2.348–2.387 Å (**9**), 2.317 Å (**5**), and 2.371 Å (**6**)) seems to be unaffected by the metal and depends mainly on the nature of the halide (Pt–Cl = 2.317 Å (**6**) vs. Pt–I = 2.600 Å (**8**)).

Table 1. Selected bond lengths and angles for complexes **5**, **6**, **8**, **9**, **10**, and **12**.

| | Platinum(II) | | | | Gold(I) | |
|-----------|--------------|-----------------|-----------------|----------------------------------|-----------|-----------|
| | 5 | 6 | 8 | 9 | 10 | 12 |
| M-X [Å] | 2.372 | 2.317 | 2.600 | 2.348–2.387 | 2.275 | - |
| M-L [Å] | 1.964 | 2.022 | 2.018 | 2.031–2.041 * 1.987–1.998 # | 1.975 | 2.016 |
| L-M-L [°] | 94.22 | 180.00 | 180.00 | 173.31–175.30 * 91.00–95.42 # | - | 177.19 |
| L-M-X [°] | 94.22 | 89.55– 90.45 | 89.53– 90.47 | 177.61–177.76 * 86.21–89.12 # | 178.67 | - |

*/# moieties which are *trans* (*) or *cis* (#) configured to each other; X = Cl (**5**, **8**, **9**, **10**) or I (**8**).

The [AuLCl] complex (**10**) formed slightly distorted columnar structures, which are mainly due to π - π interactions between the benzimidazole moieties [51]. While for this complex a Au–Au distance in the range of 6 Å could be determined, which corresponds to the minimal distance necessary for aurophilic interactions, all the other crystalized complexes have shown no metal–metal interactions (>7.8 Å).

For *trans*-[PtL₂X₂] complexes (X = Cl (**6**), I (**8**)), the ligands organized themselves into a formation in which the NHC moieties are perpendicularly arranged relative to the plane coordination sphere of the platinum(II) (Figure 3). In the case of [AuL₂]⁺ (**12**), *cis*-[PtL₂Cl₂] (**5**), and [PtL₃Cl]⁺ (**9**), a twisted alignment of the NHC moieties to each other over the metal center can be observed (Figures 2 and S29). In contrast, the NHC ligands adopted a completely planar alignment in the *trans*-[PtL₂X₂] complexes **6** and **8** due to the steric repulsion with the two halido ligands. This spatial arrangement can also be observed in similar isoelectronic gold(III) complexes with benzimidazol-2-ylidene ligands [54].

2.3. Stability in Organic Solvents and Cell Culture Medium

All metal NHC complexes under investigation exhibited a very limited water solubility. However, gold complexes **10**–**12** and the tris(carbene) platinum complex **9** were well soluble in common organic solvents, such as ACN, DMSO, DMF, and DCM. The solubility of the other Pt(II)–NHC complexes depends on their configuration. The *trans*-configured complexes **6** and **8** were poorly soluble in all solvents tested. Only DCM or CHCl₃ allowed the preparation of solutions at concentrations of about 1 mg/mL, suitable for the measurement of NMR spectra (solvent: CDCl₃). However, both solvents are inappropriate for *in vitro* experiments. Therefore, complexes **6** and **8** were omitted from the cell culture experiments.

The stability of the compounds in DMF, DMSO, and ACN was assessed by means of RP-HPLC to verify the suitability of these solvents for the preparation of stock solutions for biological experiments.

It is well known that solvent molecules (such as DMSO) can attack the platinum as nucleophiles and exchange the leaving group(s) in platinum(II) complexes [43,55–59]. Expectedly, Pt(II)–NHC compounds, in contrast to their gold counterparts (data not shown), were not inert toward DMSO and slow degradation was observed over an incubation period of 72 h (Figures S31–S33). The cationic tris(carbene) complex **9** possessed the highest stability in DMSO with more than 80% of the complex remaining intact after 72 h (Figure S33).

All investigated compounds were stable in DMF (see Figure S34), confirming the suitability of this solvent for subsequent cell culture experiments. They were also stable in a 50:50 (*v/v*) mixture of DMF/water, as exemplary shown for complex **9** (Figure S35). With the exception of **7**, the complexes could be stored in ACN without degradation (Figure S35). In the case of **7**, a slow time-dependent degradation took place (only 70% of complex remained intact after 72 h of incubation) (see Figure S36). ACN has already proven its suitability as a solvent for reactivity studies of Au(I/III)–NHC complexes in previous projects [39,43–45]. On the one hand, it can be mixed well with water (with or without

additives such as Cl^- or other nucleophiles) and, on the other hand, it does not produce any interfering solvent signals in the chromatograms obtained with our RP-HPLC method.

As a next step, the stability of the complexes in the presence of cell culture medium was examined. Therefore, compounds **5**, **7**, and **9–12** were dissolved in ACN, diluted with RPMI 1640 (without fetal calf serum (FCS)) in a 50:50 (*v/v*) ratio, and monitored by RP-HPLC over 72 h of incubation at rt. The results from the study are summarized in Figures 4 and S38–S43.

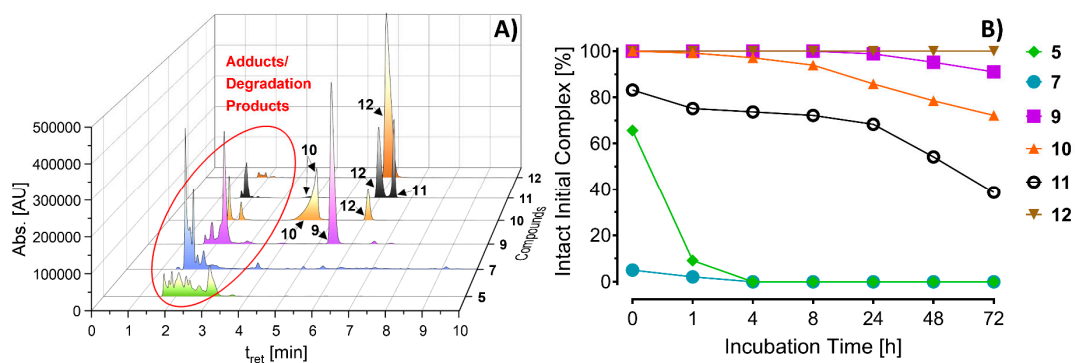


Figure 4. Time-dependent stability of compounds **5**, **7**, and **9–12** in ACN/RPMI 1640 (w/o FCS) = 50:50 (*v/v*). (A) HPLC chromatograms at $t_{72\text{h}}$. (B) Decrease of the amounts of initial complex over 72 h of incubation at rt as calculated from the chromatograms recorded at 254 nm. Complex concentration: 0.5 mM.

Platinum complexes **5** and **7** showed fast decomposition in ACN/RPMI mixture to a variety of degradation products, which were not further characterized. Time-dependent analysis indicated that less than 10% of **5** remained intact after 1 h (Figure S38), while **7** reacted instantly with ingredients of the medium (Figure S39). The tris(carbene) platinum complex **9** proved to be stable in the experimental setting used, with more than 90% of the parent compound remaining intact after 72 h (see Figure S43).

The $[\text{AuL}_2]^+$ complex **12** showed an overall higher stability than the platinum derivatives. No signs of decomposition could be observed over 72 h of incubation (Figures 5 and S40). In the case of $[\text{AuLI}]$ **11**, a fast I/Cl exchange to **10** (12.3%) and ligand scrambling to **12** (4.5%) already took place at $t = 0$ h. In the course of 72 h, the proportions changed to 58.2% **12** and 3.1% **10**, respectively (Figure S41). For $[\text{AuLCl}]$ **10**, besides the transformation to **12** (1.0% at $t = 4$ h \rightarrow 18.7% at $t = 72$ h), a slow glutathione (GSH) adduct formation from 0.8% at $t = 1$ h to 9.1% at $t = 72$ h could be observed (Figure S42). These findings are well comparable with the data obtained for other Au(I)–NHC complexes [45].

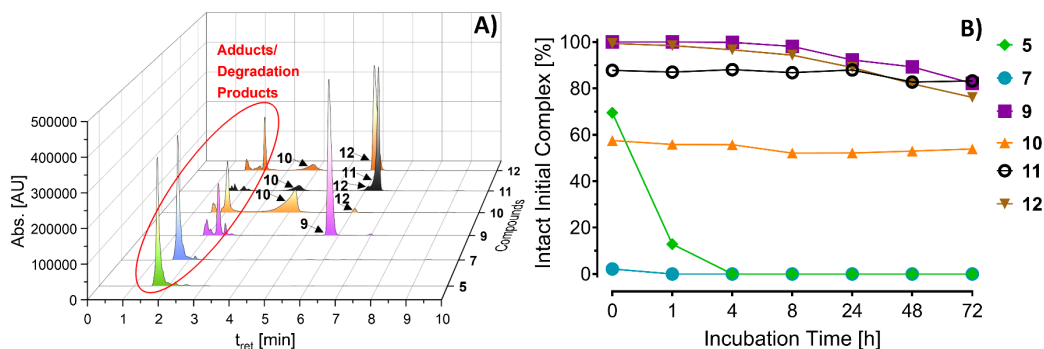


Figure 5. Reactivity of compounds **5**, **7**, and **9–12** (0.5 mM) toward GSH (5 equiv.) in ACN/PBS (pH 7.4) = 50:50 (*v/v*). (A) HPLC chromatograms at $t_{72\text{h}}$. (B) Decrease of initial complex over 72 h of incubation at rt as calculated from the chromatograms recorded at 254 nm.

2.4. Reactivity toward GSH and 5'-Guanosine Monophosphate (5'-GMP)

The time-dependent reactivity of the Pt(II)/Au(I)-NHC complexes **5**, **7**, and **9–12** toward the biologically relevant nucleophiles GSH and 5'-GMP at physiological pH (PBS, pH 7.4) have been investigated to gain further insights into the mechanism of action of the compounds. The RP-HPLC method used allowed the discrimination of formed adducts/degradation products from the initial complexes.

GSH is a strong nucleophile and reducing agent present in the human body that is known to react with metal complexes and is, to a large extent, responsible for the cellular deactivation of cisplatin [60]. The results from the incubation experiments conducted with complexes **5**, **7**, and **9–12** (0.5 mM) with GSH (5 equiv.) in ACN/PBS (pH 7.4) = 50:50 (*v/v*) are depicted in Figure 5, as well as in Figures S44–S52.

The [AuLCl] complex (**10**) reacted with GSH with adduct formation of 42.5% already at $t = 0$ h. This amount remained unchanged over the observed time period (72 h). Of the remaining unbound complex (57.5%), 3.6% transformed to **12** via ligand scrambling during a period of 72 h (see Figure S44). An exchange of PBS to water led to a complete formation of the GSH adduct at $t = 0$ h (Figure S45). Complex **11** proved to be relatively stable against a GSH attack. After 72 h, 2.7% of the GSH adduct, 9.5% of [AuLCl] (**10**), and 4.5% of [AuL₂]⁺ (**12**) were formed (see Figure S46). These results coincide with recent observations for related [Au(NHC)Cl/I] complexes [45].

Interestingly, the cationic [AuL₂]⁺ complex **12** showed some reactivity towards GSH, in contrast to previous observations for such type of compound [39,45,61,62]. After 1 h, a peak, which could be assigned to the free ligand, was detected. Its amount increased from 1.5% to 8.2% over 72 h. After 24 h, the chlorido complex **10** and the GSH adduct were also present at amounts of 3.2% and 1.3%, respectively. Their amounts increased to 6.6% and 2.0% after 72 h (see Figure S47). When the experiment was repeated in ACN/water, no degradation of **12** occurred (see Figure S48). This suggests that the minimal amounts of free ligand, complex **10**, and its GSH adduct observed in the ACN/PBS setting are caused by the high concentration of Cl[−] in the solution [45].

The neutral platinum complexes *cis*-[PtL₂Cl₂] (**5**) and *cis*-[PtL₂I₂] (**7**) rapidly reacted with GSH in ACN/PBS solution. At $t = 0$ h, only 68.5% of **5** and 2.2% of **7** were detectable in the chromatograms. A complete degradation of **5** was observed after 4 h (Figure S49) and in the case of **7** after 1 h (Figure S50).

The tris(carbene) complex **9** proved to be more stable under the conditions used. A slow degradation started at $t = 4$ h; after 72 h, 82.15% of the complex was still intact (Figures 5 and S51). The high chloride concentration in PBS diminished the coordination of GSH to platinum because, in ACN/water, GSH exchanged the Cl[−] leaving group within 24 h by 76.3% and sustained this amount during the incubation to $t = 72$ h (Figure S52).

Since DNA is regarded as one of the main targets for platinum(II) containing drugs [63–66], it is also of interest to investigate the DNA binding activity of the Pt(II)-NHC complexes of the benzimidazol-2-ylidene type and their corresponding Au(I)-NHC analogs. The reaction with the nucleotide 5'-GMP is a simple and commonly used model to assess the ability of metal complexes to coordinate to DNA bases. Accordingly, compounds **5**, **7**, and **9–12** were incubated with 5'-GMP (5 equiv.) in ACN/PBS (pH 7.4) = 50:50 (*v/v*) and potential reaction products were monitored via RP-HPLC over 72 h.

None of the Au(I)-NHC complexes showed interaction with 5'-GMP (Figures 6 and S53–S60). Even in a chloride-free ACN/water mixture, complex **10** did not interact with 5'-GMP (see Figure S56). In case of complex **11**, I/Cl exchange (\rightarrow **10**: 9.9% after 72 h) and ligand scrambling to **12** (15.9% after 72 h) was observed (see Figures 6 and S54).

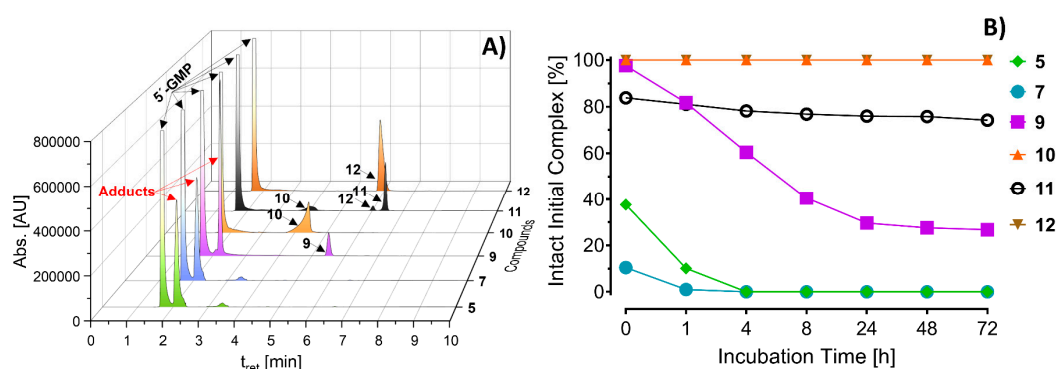


Figure 6. Reactivity of compounds 5, 7, and 9–12 (0.5 mM) toward 5'-GMP (5 equiv.) in ACN/PBS (pH 7.4) = 50:50 (*v/v*). (A) HPLC chromatograms at t_{72h} . (B) Decrease of initial complex over 72 h of incubation at rt as calculated from the chromatograms recorded at 254 nm.

The Pt(II)–NHC complexes 5 and 7 rapidly reacted with 5'-GMP (>60% already at $t = 0$ h), and the parent compounds could no longer be detected after 4 h of incubation. A third NHC ligand slowed down the reaction kinetic. After 4 h of incubation, more than 60% of the tris(carbene) complex 9 was still detectable. This amount decreased to 29.7% after 24 h, reaching a plateau (see Figure S59). The dependence of the reaction kinetic on the presence of chloride was again demonstrated in this experiment. The exchange of PBS to water led to a faster reaction with a complete disappearance of the parent compound after 24 h (Figure S60). These incubation experiments suggest that the new tris(carbene) complex 9 interacts faster with 5'-GMP compared to GSH. This presumption was also confirmed in a competitive experiment where 9 was co-incubated with equal amounts of 5'-GMP and GSH in ACN/water = 50:50 (*v/v*) (Figure S61).

2.5. Interference with Double Stranded Plasmid-DNA

The cell-free double stranded (ds) DNA plasmid electrophoretic assay is a straightforward method to obtain some preliminary insight into a compound's capacity for interacting with DNA. All interfering effects of medium constituents and influences of cellular accumulation or defense mechanisms are excluded, and the direct impact of the compounds on pSPORT1 plasmid dsDNA can be examined.

DMF, which served as a vehicle for dissolving the evaluated complexes, was tested as a control (labeled as DMF in Figure 7). The resulting electropherogram was comparable to untreated controls, indicating that DMF has no influence on the DNA plasmid. Only a somewhat intensified band corresponding to an open circular plasmid was observed, which might suggest a certain incidence of single strand breaks. This solvent effect, however, does not have an impact on the interaction of Pt(II)/Au(I)–NHC complexes (conc. 15 μ M) with the supercoiled form.

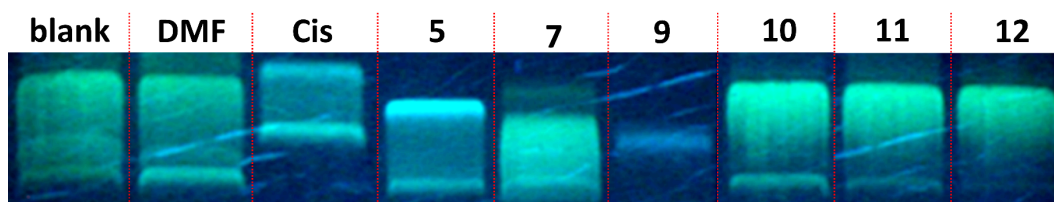


Figure 7. Electropherograms of dsDNA plasmid pSPORT1 incubated with 15 μ M of Pt(II)-/Au(I)-NHC compounds 5, 7, and 9–12, cisplatin (Cis), DMF (vehicle control), and nuclease-free water (blank) after 4 h of incubation at 37 °C.

Cisplatin (Cis) caused an untwisting open circular form after 4 h of incubation, indicated by a significant DNA band shift (see Figure 7) [32,67]. The DNA band shift pattern

caused by the Pt(II)–NHC complexes strongly differ from that of cisplatin. *Cis*-[PtL₂Cl₂] (**5**) transferred the dsDNA from the supercoiled to the linear plasmid form, similar to *cis*-[PtL₂I₂] (**7**). In the latter case, however, a weak band of the supercoiled form is still present. Notably, the tris(carbene) complex **9** completely destroyed the structure of the dsDNA and only one newly formed band can be seen after 4 h of incubation. This might be the consequence of different modes of DNA binding (monofunctional (**9**) vice versa bifunctional (**5**, **7**)).

No DNA interaction could be verified for the Au(I)–NHC complexes **10–12**. The obtained bands are comparable to that of the vehicle control (DMF).

Overall, the dsDNA plasmid electrophoretic assay confirmed that the platinum species **5**, **7**, and **9** are susceptible to DNA interactions in contrast to their gold analogues **10–12**. Nevertheless, the Pt(II)–NHC complexes altered the electrophoretic mobility of DNA in a different way than cisplatin, suggesting a distinct mode of DNA binding.

2.6. In Vitro Cytotoxicity

The antiproliferative activity of the Au(I)/Pt(II)–NHC complexes (**5**, **7**, and **9–12**) was evaluated in the ovarian carcinoma cell line A2780wt and its corresponding cisplatin-resistant subvariant A2780cis. The established metallodrugs cisplatin and auranofin were also examined for comparison.

The cell lines represent the model of choice as the platinum-based drugs cisplatin or carboplatin are used in first-line chemotherapy of ovarian carcinoma [68,69]. For auranofin (and related gold complexes), promising activity against this malignancy was also documented [70,71]. Furthermore, ovarian cancer resistance to existing treatments is becoming more common [72,73] and, thus, new metallodrugs are needed for second-line therapies.

The *in vitro* cytotoxicity of the compounds was assessed using the colorimetric MTT assay to determine the metabolic activity of the cells. The obtained IC₅₀ values as well as the calculated resistance factor (RF) are summarized in Table 2 (see Figures S62 and S63 for concentration-effect curves).

Table 2. Metabolic activity in A2780wt and A2780cis cells determined with an MTT assay as well as the resulting resistance factor (RF).

| | Compound | Metabolic Activity IC ₅₀ ^a [μM] | | RF ^b x-Fold |
|--------------|------------------|---|--------------|---------------------------|
| | | A2780wt | A2780cis | |
| Ligand | 2 | >40 | >40 | - |
| Platinum(II) | 5 | >6.25 | >6.25 | - |
| | 7 | >6.25 | >6.25 | - |
| | 9 | 0.63 ± 0.18 | 1.14 ± 0.32 | 1.82 |
| | cisplatin | 0.87 ± 0.46 | 10.56 ± 2.16 | 12.17 |
| | 10 | 4.31 ± 1.29 | 6.69 ± 1.55 | 1.55 |
| Gold(I) | 11 | 1.02 ± 0.59 | 1.28 ± 0.44 | 1.25 |
| | 12 | 0.09 ± 0.05 | 0.11 ± 0.05 | 1.21 |
| | auranofin | 1.04 ± 0.49 | 2.31 ± 0.65 | 2.22 |

^a The IC₅₀ value represents the concentration causing 50% decrease in metabolic activity after 72 h of drug exposure and is calculated as the mean ± SEM of six independent experiments. ^b Resistance factor (RF), calculated as RF = IC₅₀(A2780cis)/IC₅₀(A2780wt).

The gold complexes **10–12** caused a concentration-dependent decrease of the metabolic activity in both cell lines with slightly higher IC₅₀ values obtained in the A2780cis cells. The most active compound was the cationic bis(carbene) gold complex **12** with IC₅₀ values of 0.09 μM (A2780wt) and 0.11 μM (A2780cis), respectively. This means that **12** possesses 12/21-times higher activity than auranofin and 10/96-times higher activity than cisplatin in these cell lines. These findings are in a good agreement with previous studies on [Au(NHC)₂]⁺ complexes [38,39,74,75]. Complex **11** showed a higher cytotoxicity than **10** in both cell lines, which could be the result of higher cellular accumulation and/or faster

transformation to the more active complex **12** upon ligand scrambling (see Section 2.3 and refs. [38,43,44]).

The low water solubility limited the examination of the neutral Pt(II)–NHC complexes **5** and **7**. They could only be tested up to a concentration of 6.25 μM , which was not sufficient to cause a notable decrease in cellular metabolic activity. At higher concentrations, precipitation took place upon dilution with cell culture medium. It should be mentioned that the recommended DMF concentration (<0.5%) for cell culture experiments must not be exceeded.

The tris(carbene) platinum complex **9** demonstrated high cytotoxicity with IC_{50} values in the lower micromolar range in both cell lines (0.63 μM (A2780wt) and 1.14 μM (A2780cis), respectively). Notably, this compound exhibited only a 1.82-fold decrease (vs. 12.2-fold for cisplatin) in activity on A2780cis, compared to A2780wt cells and circumvent cisplatin resistance. The distinctly higher cytotoxicity in A2780cis cells compared to cisplatin might be the consequence of a higher accumulation in the cells or, more likely, of different DNA binding properties, as demonstrated in the DNA plasmid assay (vide supra). It seems that the DNA binding of **9** is not recognized by DNA repair mechanisms.

To evaluate the selectivity toward cancer cells, compounds **5**, **7**, and **9–12** were additionally tested in human fibroblast cells. Complexes **9–12** were significantly less active in non-cancerous cells compared to A2780wt cells when tested at the same concentrations (Figure 8). As expected, the low solubility also limited the effects of **5** and **7** in fibroblasts. Comparable to A2780cis cells, no reduced viability was observed up to a concentration of 6.25 μM .

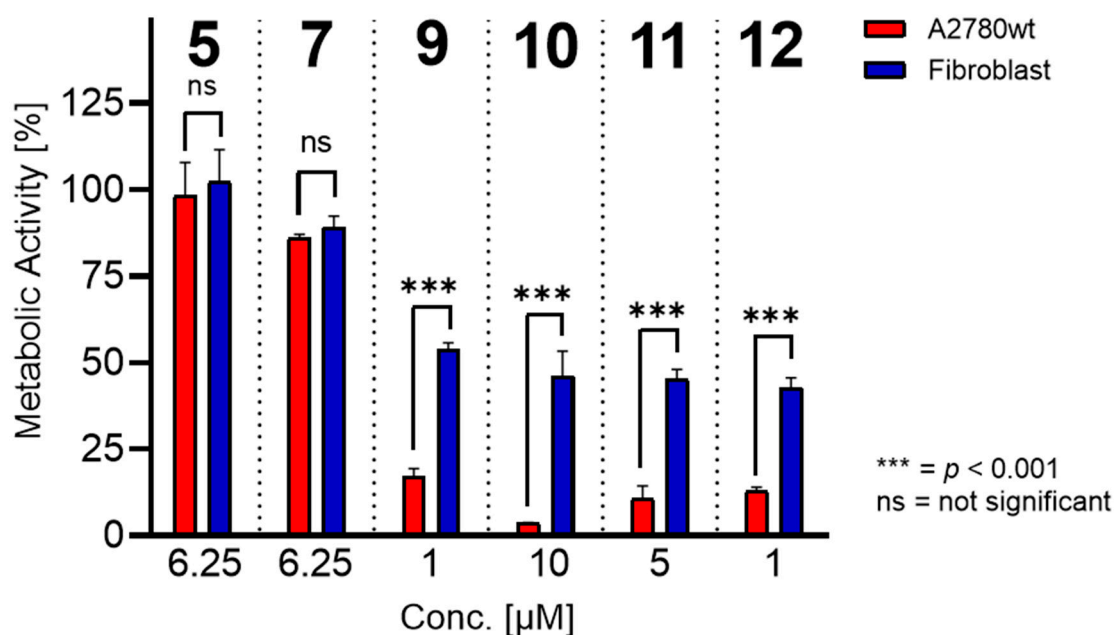


Figure 8. Metabolic activity in non-cancerous fibroblast cells vs. A2780wt cells determined in an MTT assay. Values were calculated as the mean \pm SEM of four independent experiments.

3. Materials and Methods

3.1. Materials

Chemical reagents and solvents were purchased from commercial suppliers (Sigma-Aldrich (St. Louis, MI, USA), BLDpharm (Cincinnati, OH, USA), Fluka (Buchs, Switzerland), Alfa Aesar (Ward Hill, MA, USA), and Abcr (Karlsruhe, Germany)) and were used without further purification. Thin layer chromatography was carried out on Polygram[®] SIL G/UV254 (Macherey-Nagel (Düren, Germany)) pre-coated polyester sheets; the spots were visualized by UV light (254 nm). For column chromatography, silica gel 60 (0.040–0.063 mm, VWR) was used. NMR spectra were recorded on a Bruker (Billerica,

MA, USA) Avance 4 Neo 400 MHz spectrometer at 400.13 (^1H), 100.62 (^{13}C), 161.98 (^{31}P), 376.46 MHz (^{19}F), and 85.88 (^{195}Pt) MHz in CDCl_3 or $\text{DMSO}-d_6$ (purchased at Eurisotop (Saint-Aubin, France)) at an ambient temperature. Chemical shifts (δ) are given in ppm and were referenced relative to the internal standard TMS for ^1H and ^{13}C NMR spectroscopy, external $\text{Na}_2[\text{PtCl}_6]$ for ^{195}Pt NMR spectroscopy, external H_3PO_4 for ^{31}P , and external CFCl_3 for ^{19}F NMR spectroscopy. NMR data were processed using MestreNova 14.3.0. Infrared spectra were obtained on a Bruker Alpha FT-IR-spectrometer with an ATR unit (attenuated total reflection unit) in the range of 4000–400 cm^{-1} . Intensities of the reported bands are described with s for strong, m for medium, and w for weak; broad signals are additionally specified with the letter b in front of these abbreviations. High-resolution mass spectra (HRMS) were measured with Orbitrap Elite mass spectrometer (Thermo Fisher Scientific, Waltham, MA, USA) using direct infusion and electrospray ionisation (ESI). Measurements were conducted in positive ion mode. MS data analysis was carried out with Xcalibur. RP-HPLC experiments (determination of purity and reactivity studies) were performed on a Shimadzu prominence HPLC system with autosampler SIL-20A HT, column oven CTO-10AS VP, degassers DGU-20A, detector SPD-M20A, pumps LC-20AD, and a reverse phase C18 column (KNAUER Eurospher 100-5 C18, 250 \times 4 mm). The mobile phase consisted of ACN (HPLC-grade) and Milli Q water (Millipore GmbH, Vienna, Austria) with 0.1% TFA. To achieve separation of the compounds, a gradient elution from 60–90% ACN/water was used with a flow rate of 1 mL/min at an oven temperature of 35 $^\circ\text{C}$. All solvents have been degassed before use. The injection volume was 20 μL and the UV-VIS detection wavelength was set at 254 nm. The software used for data processing was LabSolutions. The purity (>95%) of all bio-tested compounds was confirmed by RP-HPLC.

3.2. Synthesis

A general reaction scheme is given in Scheme 2. 1,3-Diethylbenzimidazol-2-ium iodide (**1**) was prepared from benzimidazole based on literature methods [42] with some modifications. The respective chloride (**2**) and hexafluorophosphate (**3**) analogs were obtained from **1** via salt metathesis (see the Supplementary Materials). Platinum precursor *cis*-[Pt(DMSO) $_2$ Cl $_2$] [76] as well as complex **4** [50] were synthesized as described in the literature. *Cis*-[Pt(DMSO) $_2$ I $_2$] was prepared similarly to *cis*-[Pt(DMSO) $_2$ Cl $_2$], using $\text{K}_2[\text{PtI}_4]$ (prepared *in situ* from $\text{K}_2[\text{PtCl}_4]$ and KI) instead of $\text{K}_2[\text{PtCl}_4]$ as a starting material.

3.2.1. Synthesis of Platinum Complexes (5–9)

cis-Dichlorido[bis(1,3-diethylbenzimidazol-2-ylidene)]platinum(II) (**5**)

Cis-[Pt(DMSO) $_2$ Cl $_2$] (40 mg, 95 μmol , 1 equiv.), **2** (60 mg, 280 μmol , 3 equiv.), and NaOMe (23 mg, 430 μmol , 4.5 equiv.) were dissolved/suspended under an argon atmosphere in 4 mL of anhydrous ACN. The reaction mixture was stirred at rt for 4 h under protection from light. The precipitate formed was collected via filtration, re-suspended in DCM, and filtered from undissolved inorganic salts. The volume of the filtrate was reduced by rotary evaporation, and Et_2O was added to precipitate the final product, which was collected via filtration, washed with Et_2O , and dried in vacuum to give complex **5** as almost white solid, 28 mg (48% yield). ^1H NMR (400 MHz, CDCl_3): δ 7.41–7.34 (m, 4H, Ar-H), 7.30–7.25 (m, 4H, Ar-H), 5.06 (m, 4H, CH $_2$), 4.65 (m, 4H, CH $_2$), 1.46 (t, J = 7.2 Hz, 12H). ^{13}C NMR (101 MHz, CDCl_3): δ 158.8 (NCN), 133.5 (Ar-C $_q$), 123.5 (Ar-CH), 111.0 (Ar-CH), 43.6 (CH $_2$), 14.3 (CH $_3$). ^{195}Pt NMR (86 MHz, CDCl_3): δ –3630. ESI-HRMS(+) found (calculated): m/z [M + Na $^+$] $^+$, 637.1147 (637.1188); [M + CH $_3\text{CN}-\text{Cl}$] $^+$, 619.1861 (619.1867). FT-IR (ATR, cm^{-1}): 3398 bw; 2984 bw, 2966 bw; 1479 w, 1406 m, 1266 w, 1089 w; 765 s, 550 bm. Purity was calculated using HPLC (peak area): 97.5%. Characterization also in the literature [52].

trans-Dichlorido[bis(1,3-diethylbenzimidazol-2-ylidene)]platinum(II) (**6**)

Complex **6** was prepared by a similar procedure as described for related compounds [52]. A total of 106 mg (500 μmol , 2 equiv.) of **2** was dissolved in 30 mL of anhydrous DCM and treated with Ag_2O (83 mg, 356 μmol , 1.4 equiv.). The mixture was stirred for 12 h at rt and

under the exclusion of light. Then, 108 mg (262 μmol , 1 equiv.) of pulverized $\text{K}_2[\text{PtCl}_4]$ was added and the reaction mixture was stirred for an additional 7 days. After filtration over a pad of celite, the filtrate was concentrated under reduced pressure, and Et_2O was added to precipitate the crude product. The latter was purified via column chromatography (DCM/MeOH = 12:1) and recrystallization from DCM to yield complex **6** as almost white solid, 50 mg (34% yield). ^1H NMR (400 MHz, CDCl_3): δ 7.48–7.39 (m, 4H, Ar-H), 7.34–7.26 (m, 4H, Ar-H), 4.97 (q, $J = 7.3$ Hz, 8H, CH_2), 1.76 (t, $J = 7.3$ Hz, 12H, CH_3). ^{13}C NMR (101 MHz, CDCl_3): δ 178.2 (NCN), 134.0 (Ar- C_q), 122.8 (Ar-CH), 110.3 (Ar-CH), 42.4 (CH_2), 15.0 (CH_3). ^{195}Pt NMR (86 MHz, CDCl_3): δ –3252. ESI-HRMS(+) found (calculated): m/z $[\text{M} + \text{Na}^+]^+$, 637.1180 (637.1188). FT-IR (ATR, cm^{-1}): 2969 bw, 2934 bw; 1450 w, 1412 m, 1223 w, 1093 w; 763 s.

***cis*-Diiodido[bis(1,3-diethylbenzimidazol-2-ylidene)]platinum(II) (7) and *trans*-Diiodido[bis(1,3-diethylbenzimidazol-2-ylidene)]platinum(II) (8)**

Cis- $[\text{Pt}(\text{DMSO})_2\text{I}_2]$ (121 mg, 199 μmol , 1 equiv.), **1** (151 mg, 499 μmol , 2.5 equiv.), and NaOtBu (61 mg, 635 μmol , 3.2 equiv.) were dissolved/suspended under an argon atmosphere in 18 mL of anhydrous DCM. The reaction mixture was stirred at rt for 30 h and under protection from light. The precipitate formed was collected via filtration, re-suspended in water, filtered, washed with MeOH and Et_2O , and dried in vacuum to give complex **8** as a pale yellow solid (32 mg). The volume of the filtrate was reduced by rotary evaporation to approx. 1–2 mL and the newly formed precipitate was collected via filtration. The latter was subjected to column chromatography with DCM as a mobile phase to obtain pure complex **7** (68 mg) and complex **8** (10 mg).

Complex **7**: almost white solid, 68 mg (43% yield). ^1H NMR (400 MHz, CDCl_3): δ 7.41–7.33 (m, 4H, Ar-H), 7.28–7.24 (m (superimposed by the solvent peak), 4H, Ar-H), 5.21 (m, 4H, CH_2), 4.56 (m, 4H, CH_2), 1.58 (t, $J = 7.2$ Hz, 12H). ESI-HRMS(+) found (calculated): m/z $[\text{M}-\text{I}^-]^+$, 670.0944 (670.0958); $[\text{M} + \text{CH}_3\text{CN}-\text{I}^-]^+$, 711.1214 (711.1223). FT-IR (ATR, cm^{-1}): 2977 bw, 2931 bw; 1478 w, 1396 m, 1261 w, 1086 w; 751 s, 568 w. Purity was calculated using HPLC (peak area): 95.5%.

Complex **8**: pale yellow solid, 42 mg (27% yield). ^1H NMR (400 MHz, CDCl_3): δ 7.44–7.37 (m, 4H, Ar-H), 7.30–7.26 (m, 4H, Ar-H), 4.86 (q, $J = 7.3$ Hz, 8H, CH_2), 1.71 (t, $J = 7.3$ Hz, 12H, CH_3). ^{13}C NMR (101 MHz, CDCl_3): δ 122.6 (Ar-CH), 110.3 (Ar-CH), 42.8 (CH_2), 14.1 (CH_3). IR (ATR, cm^{-1}): 2975 bw, 2932 bw; 1478 w, 1408 m, 1257 w, 1091 w; 758 s, 569 w.

Chlorido[tris(1,3-diethylbenzimidazol-2-ylidene)]platinum(II) hexafluorophosphate (9)

• Method A

Cis- $[\text{Pt}(\text{DMSO})_2\text{Cl}_2]$ (124 mg, 293 μmol , 1 equiv.), **3** (300 mg, 937 μmol , 3.2 equiv.), NaOtBu (99 mg, 1002 μmol , 3.5 equiv.), and KPF_6 (108 mg, 586 μmol , 2 equiv.) were dissolved/suspended in 10 mL of anhydrous DCM in a high pressure tube and stirred at 40 °C for 48 h. Subsequently, the mixture was filtered over a pad of celite, the volume of the filtrate was reduced by rotary evaporation, and Et_2O was added to precipitate the crude product. The latter was purified by column chromatography (DCM/MeOH = 12:1), followed by double recrystallization from MeOH and washing with Et_2O yielding **9**, a white solid, 12 mg (11% yield). ^1H NMR (400 MHz, CDCl_3): δ 7.51–7.41 (m, 4H, Ar-H), 7.46–7.42 (m, 2H, Ar-H'), 7.38–7.33 (m, 4H, Ar-H), 7.32–7.28 (m, 2H, Ar-H'), 4.96 (m, 4H, CH_2), 4.84 (q, $J = 7.2$ Hz, 4H, CH_2'), 4.65 (m, 4H, CH_2), 1.45 (t, $J = 7.2$ Hz, 12H, CH_3), 0.68 (t, $J = 7.2$ Hz, 6H, CH_3'). ^{13}C NMR (101 MHz, CDCl_3): δ 176.6 (NCN), 154.9 (NCN'), 133.5 (Ar- C_q), 133.0 (Ar- C_q'), 124.7 (Ar-CH'), 124.2 (Ar-CH), 111.7 (Ar-CH'), 111.6 (Ar-CH), 43.9 (CH_2), 43.5 (CH_2'), 14.5 (CH_3), 13.1 (CH_3'). ^{31}P NMR (162 MHz, CDCl_3): δ –144.3 (septet, $^2J_{\text{P-F}} = 711$ Hz). ^{19}F NMR (376 MHz, CDCl_3): δ –73.2 (d, $^2J_{\text{P-F}} = 711$ Hz). ^{195}Pt NMR (86 MHz, CDCl_3): δ –3925. ESI-HRMS(+) found (calculated): m/z $[\text{M}-\text{PF}_6^-]^+$, 752.2853 (752.2807). FT-IR (ATR, cm^{-1}): 2984 bw, 2942 bw; 1481 w, 1406 m; 1261 w, 1089 w; 836 bs ($\nu_{\text{P-F}}$); 744 s, 556 s. Purity was calculated using HPLC (peak area): 98.0%

- Method B

Complex **4** (25 mg, 48 μmol , 1 equiv.), **3** (39 mg, 120 μmol , 2.5 equiv.), NaOMe (13 mg, 240 μmol , 5 equiv.), and KPF_6 (27 mg, 140 μmol , 3 equiv.) were dissolved/suspended in 3 mL of anhydrous DCM and stirred at 30 °C for 24 h. Subsequently, the mixture was filtered over a pad of celite, the volume of the filtrate was reduced by rotary evaporation, and Et_2O was added to precipitate the crude product. The latter was purified by column chromatography (DCM/MeOH = 12:1), followed by recrystallization from MeOH and washing with Et_2O yielding **9** as an almost white solid, 14 mg (32% yield). Purity was calculated using HPLC (peak area): 95.4%

3.2.2. Synthesis of Gold Complexes (10–12)

Complexes **10–12** [51] were prepared according to procedures previously established in our group [39], which allow straightforward isolation of the products in high purity and yield.

Chlorido[1,3-diethylbenzimidazol-2-ylidene]gold(I) (10)

A total of 125 mg (390 μmol , 1 equiv.) of **3** was dissolved under an argon atmosphere and exclusion of light in an anhydrous DCM/MeOH (3 + 3 mL) mixture and supplemented with 64 mg (273 μmol , 0.7 equiv.) of Ag_2O . The resulting suspension was stirred overnight (12 h) at rt. Then, 83 mg (1.952 mmol, 5 equiv.) of LiCl was added to the reaction mixture together with 126 mg (429 μmol , 1.1 equiv.) of $[\text{Au}(\text{S}(\text{Me})_2)\text{Cl}]$. After stirring for additional 6 h and evaporating of the solvent, the residue was purified by column chromatography (DCM/MeOH = 9.8:0.2). The final product **10** was obtained after recrystallization from *n*-pentane as an off-white solid, 80 mg (50% yield). ^1H NMR (400 MHz, CDCl_3): δ 7.50–7.47 (m, 2H, Ar-H), 7.47–7.42 (m, 2H, Ar-H), 4.54 (q, $J = 7.3$ Hz, 4H, CH_2), 1.53 (t, $J = 7.3$ Hz, 6H, CH_3). ^{13}C NMR (101 MHz, CDCl_3): δ 177.4 (NCN), 132.8 (Ar- C_q), 124.4 (Ar-CH), 111.4 (Ar-CH), 44.0 (s, CH_2), 15.5 (s, CH_3). ESI-HRMS(+) found (calculated): m/z $[\text{M} + \text{ACN} - \text{Cl}]^+$, 412.1101 (412.1088). FT-IR (ATR, cm^{-1}): 2982 w, 2928 bw; 1459 m; 1410 m, 1084 w; 740 s, 566 w. Purity was calculated using HPLC (peak area): 99.4%. Detailed characterization also in the literature [51].

Iodido[1,3-diethylbenzimidazol-2-ylidene]gold(I) (11)

A total of 25 mg (61 μmol , 1 equiv.) of **10** was dissolved in 5 mL of anhydrous acetone and stirred together with 92 mg (614 μmol , 10 equiv.) NaI for 8 min at rt. The solvent was removed under reduced pressure, and the residue was taken up in DCM and subsequently filtered through a pad of celite to separate the remaining salts (NaI/NaCl) from **11**. The filtrate was evaporated to dryness and recrystallized from *n*-pentane to yield **11** as a yellow solid, 22 mg (88% yield). ^1H NMR (400 MHz, CDCl_3): δ 7.51–7.48 (m, 2H, Ar-H), 7.47–7.26 (m, 2H, Ar-H), 4.56 (q, $J = 7.2$ Hz, 4H, CH_2), 1.55 (t, $J = 7.3$ Hz, 6H, CH_3). ^{13}C NMR (101 MHz, CDCl_3): δ 187.1 (NCN), 132.7 (Ar- C_q), 124.5 (Ar-H), 111.4 (Ar-H), 43.6 (CH_2), 15.5 (CH_3). ESI-HRMS(+) found (calculated): m/z $[\text{M} + \text{ACN} - \text{I}]^+$, 412.1088 (412.1088). FT-IR (ATR, cm^{-1}): 2960 bw, 2922 bm; 1480 m, 1446 m, 1407 m, 1082 m; 740 s, 562 m. Purity was calculated using HPLC (peak area): 98.9%. Characterization also in the literature [51].

Bis[1,3-diethylbenzimidazol-2-ylidene]gold(I) hexafluorophosphate (12)

A total of 200 mg (625 μmol , 1 equiv.) of **3** was dissolved under an argon atmosphere and exclusion of light in an anhydrous DCM/MeOH (3 + 3 mL) mixture and supplemented with 101 mg (437 μmol , 1.4 equiv.) of Ag_2O . The resulting suspension was stirred overnight (12 h) at rt. Then, 92 mg (312 μmol , 1 equiv.) of $[\text{Au}(\text{S}(\text{Me})_2)\text{Cl}]$ was added and the mixture was stirred for another 120 h. After evaporating of the solvent, the residue was purified by column chromatography (DCM/MeOH = 9.8:0.2) to remove remaining ligand or eventually formed **10**. After recrystallization with *n*-pentane, the pure complex **12** was collected as a yellowish solid, 125 mg (64% yield). ^1H NMR (400 MHz, CDCl_3): δ 7.61–7.55 (m, 4H, Ar-H), 7.51–7.26 (m, 4H, Ar-H), 4.64 (q, $J = 7.3$ Hz, 8H, CH_2), 1.65 (t, $J = 7.3$ Hz, 12H, CH_3). ^{13}C NMR (101 MHz, CDCl_3): δ 189.6 (NCN), 133.0 (Ar- C_q), 125.0 (Ar-C), 111.66 (Ar-C), 44.04 (CH_2), 16.01 (CH_3). ^{31}P NMR (162 MHz, CDCl_3): δ -144.36 (septet, $^2J_{\text{F-P}} = 710$ Hz). ^{19}F NMR (376 MHz, CDCl_3): δ -73.6 (d, $^2J_{\text{P-F}} = 712$ Hz). ESI-HRMS(+) found (calculated):

m/z $[M-PF_6^-]^+$, 545.1988 (545.1979). FT-IR (ATR, cm^{-1}): 2963 w, 2923 bm; 1480 m, 1420 m, 1089 w; 827 bs (ν_{P-F}); 766 s, 556 s. Purity was calculated using HPLC (peak area): 99.7%. Characterization also in the literature [51].

3.3. HPLC Investigations

To investigate the stability of the complexes in pure organic solvents (ACN, DMF, and DMSO), 0.5 mM solutions were used. For the other stability studies, DMF or ACN stocks of the respective compounds (1.0 mM) were prepared and diluted with Milli Q water or RPMI 1640 (w/o FCS) 50:50 (v/v), respectively.

For experiments with relevant biomolecules (5'-GMP, GSH), an ACN/PBS (or water) mixture was prepared as follows: a 1.0 mM stock solution of the respective complex was made in ACN and diluted 50:50 (v/v) with PBS (water) solution containing 5.0 mM GSH or 5'-GMP to reach a final concentration of 0.5 mM complex and 2.5 mM GSH or 5'-GMP, respectively.

All the solutions were incubated for 72 h at rt. Samples (20 μ L each) were taken at appropriate time points ($t = 0$ h (1.5 min), 1 h, 4 h, 8 h, 24 h, 48 h, and 72 h) and analyzed via RP-HPLC (see Section 3.1). The chromatograms were displayed with the program Origin Pro 2018 (Origin Lab Corporation, Northampton, MA, USA).

3.4. X-ray Crystallography

For single crystal structure analysis, crystals were measured into a stream of cold N_2 inside a Bruker D8 Quest diffractometer (Photon III C14). The instrument was equipped with an Incoatec Microfocus source generator (multi layered optics monochromatized Mo- K_α radiation, $\lambda = 71.073$ pm). Multi-scan absorption corrections were applied with the program SADABS-2014/5. SHELXT and SHELXL programs [77,78] were used for structure solution and refinement. Further details about crystal data, data collection parameters, and structure refinement are given in the Supplementary Materials (see Tables S1–S7). CCDC 2267764-2267770 contains additional crystallographic data for this paper. These data can be obtained free of charge from the Cambridge Crystallographic Data Centre.

3.5. Electrophoretic Double Stranded DNA Plasmid Assay

A total of 2 μ L (conc. 0.5 μ g/ μ L) of pSport1 (4109 bp) plasmid was mixed with 2 μ L of each test compound (150 μ M in DMF) and diluted with 16 μ L of nuclease-free water to reach a final concentration of 15 μ M. Subsequently, this mixture was incubated for 4 h at 37 °C under gentle shaking. Samples were loaded with gel loading buffer on an agarose gel (0.5% (w/v) in $1 \times$ Tris-acetate-EDTA (TAE) buffer + 0.004% Midori Green Advance). The following running parameters were used: 95 min at 3 V/ cm^{-1} in $1 \times$ TAE buffer. Images were visualized under UV light (254 nm).

3.6. Cell Lines

The ovarian carcinoma cell lines A2780wt and A2780cis were kindly provided by the Department of Gynaecology, Medical University, Innsbruck. To maintain resistance, A2780cis cells were incubated fortnightly with 1 μ M of cisplatin. The fibroblasts were kindly provided by the Department of Internal Medicine V, Medical University Innsbruck. The cell lines and the fibroblasts were cultivated in RPMI 1640 without phenol red (BioWhittaker, Lonza, Walkersville, MD, USA), supplemented with L-glutamine (2 mM), FCS (10%) (all from Invitrogen Corporation, Gibco, Paisley, UK), Penicillin (100 U mL^{-1}), and Streptomycin (100 μ g mL^{-1}) at 37 °C in a 5% CO_2 /95% air-humidified atmosphere, and fed/passaged twice weekly.

3.7. Cytotoxicity Assays and Data Analysis

The exponentially growing cells were seeded at a density of 8000 cells/well (A2780wt, A2780cis, and fibroblasts) into clear flat-bottom 96-well plates in triplicates. Following 24 h of incubation at 37 °C in a humidified atmosphere (5% CO_2 /95% air), stock solutions of

the test compounds were prepared in DMF, serially diluted with completed medium to the respective concentrations, and added to the cells (final DMF content did not exceed 0.5%). After another 72 h of incubation, the cellular metabolic activity was measured as an indicator of cell viability employing a 3-(4,5-dimethylthiazol-2-yl)-2,5-diphenyltetrazolium bromide (MTT) assay. An MTT solution (in PBS) at a final concentration of 0.5 mg/mL was applied and the incubation was continued for 3 h at 37 °C. After medium aspiration, 200 µL of DMSO were added to each well to dissolve the formed formazan crystals. The absorbance (A) of the solution was recorded at 570 nm and 690 nm (turbidity assessment) using the EnSpire microplate reader (Perkin Elmer, Waltham, MA, USA). Solvent-treated cells without compound served as a positive control. Metabolic activity was calculated by the following equation:

$$\text{Metabolic Activity \%} = \left[\frac{A_T (\text{sample})}{A_T (\text{control})} \right] \times 100$$

$$A_T = A_{570 \text{ nm}} - A_{690 \text{ nm}}$$

The IC₅₀ values were calculated with GraphPad Prism 8.0 (GraphPad Software, Boston, MA, USA) using nonlinear regression. Data were analyzed by ordinary one-way ANOVA test (after normal distributions of data were verified by the Shapiro–Wilk test). Statistical significance was set at $p < 0.05$. Significance levels of $p < 0.001$ are denoted in the graphs by a triple asterisk.

4. Conclusions

A series of Pt(II)– and Au(I)–NHC complexes of the benzimidazol-2-ylidene type were synthesized and characterized in detail by various techniques. To elucidate the role of the metal center on the physicochemical and biological properties of the compounds, their stability in cell culture medium and in the presence of relevant biomolecules as well as their *in vitro* cytotoxicity and interactions with plasmid DNA were investigated. *Trans*-configured platinum complexes **6** and **8** displayed very poor solubility and could not be included in the studies.

Cationic [PtL₃Cl]⁺ and [AuL₂]⁺ complexes (**9** and **12**) exhibited high stability in cell culture medium with > 90% of the complex remaining intact after 72 h of incubation. In contrast, neutral platinum species **5** and **7** showed fast decomposition in this experimental setting and the parent compounds were no longer detectable after 4 h. The [AuLCl/I] complexes **10** and **11** showed chloride-dependent adduct formation with GSH and, to some extent, ligand scrambling to **12**.

Complexes **9** and **12** displayed the highest cytotoxic activity in this series on both wild-type and cisplatin-resistant ovarian carcinoma cell lines with IC₅₀ values in the low micromolar range. Notably, these compounds were capable of circumventing acquired resistance to cisplatin in the model used and showed selectivity toward cancer cells compared to non-cancerous fibroblasts. The lower activity (IC₅₀ > 6.25 µM) observed for the other platinum species tested (**5** and **7**) could be related to their low stability in biological media and solubility limitations.

Finally, all the Pt(II)–NHC complexes tested formed 5'-GMP adducts under physiologically relevant conditions and interacted with dsDNA, in contrast to their Au(I) analogs, supporting distinct mechanisms of action dependent on the metal center.

The results obtained in this study suggest that complex **12** and the new tris(carbene) compound **9** represent promising lead structures for further optimization as anticancer drug candidates. Furthermore, obtaining better water-soluble NHC complexes is necessary to facilitate the subsequent preclinical development of this type of compounds and is part of a forthcoming project.

Supplementary Materials: The following supporting information can be downloaded at: <https://www.mdpi.com/article/10.3390/inorganics11070293/s1>, Figures S1–S7: HPLC chromatograms of **2**, **5**, **7**, and **9–12** dissolved in ACN; Figures S8–S17: ^1H NMR spectra of **2** and **4–12** recorded in CDCl_3 ; Figures S18–S25: ^{13}C NMR spectra of **2**, **4–6**, and **9–12** recorded in CDCl_3 ; Figure S26: ^{195}Pt NMR spectra of **5**, **6**, and **9** recorded in CDCl_3 ; Figure S27: ESI-HRMS spectrum of **9**; Figures S28–S30: X-ray structures of **1**, **5**, and **10**; Tables S1–S7: Crystal data and structure refinement for **1**, **5**, **6**, **8–10**, and **12**; Figures S31–S33: HPLC chromatograms of **5**, **7**, and **9** incubated in DMSO up to 72 h; Figure S34: HPLC chromatograms of complexes **5**, **7**, **9**, **10**, and **12** in DMF upon 72 h of incubation; Figure S35: HPLC chromatograms of **9** incubated in DMF/water = 50:50 (*v/v*) up to 72 h; Figure S36: HPLC chromatograms of complexes **5**, **7**, **9**, **10**, and **12** in ACN at *t* = 72 h incubation time; Figure S37: HPLC chromatograms of **7** incubated in ACN up to 72 h; Figures S38–S43: HPLC chromatograms of **5**, **7**, and **9–12** over 72 h of incubation in ACN/RPMI 1640 (w/o FCS) = 50:50 (*v/v*); Figures S44 and S45: HPLC chromatograms up to 72 h incubation time of **10** dissolved in ACN/PBS(or water) = 50:50 (*v/v*) in the presence of 5 eq. GSH (red.); Figures S46 and S47: HPLC chromatograms up to 72 h incubation time of **11** and **12** dissolved in ACN/PBS = 50:50 (*v/v*) in the presence of 5 eq. GSH (red.); Figure S48: HPLC chromatograms up to 72 h incubation time of **12** dissolved in ACN/water = 50:50 (*v/v*) in the presence of 5 eq. GSH (red.); Figures S49–S51: HPLC chromatograms up to 72 h incubation time of **5**, **7**, and **12** dissolved in ACN/PBS = 50:50 (*v/v*) in the presence of 5 eq. GSH (red.); Figure S52: HPLC chromatograms up to 72 h incubation time of **9** dissolved in ACN/water = 50:50 (*v/v*) in the presence of 5 eq. GSH (red.); Figures S53–S55: HPLC chromatograms up to 72 h incubation time of **10–12** dissolved in ACN/PBS = 50:50 (*v/v*) in the presence of 5 eq. 5'-GMP (at pH 7.4); Figure S56: HPLC chromatograms up to 72 h incubation time of **10** dissolved in ACN/water = 50:50 (*v/v*) in the presence of 5 eq. 5'-GMP (at pH 7.4); Figures S57–S59: HPLC chromatograms up to 72 h incubation time of **5**, **7**, and **9** dissolved in ACN/PBS = 50:50 (*v/v*) in the presence of 5 eq. 5'-GMP (at pH 7.4); Figure S60: HPLC chromatograms up to 72 h incubation time of **9** dissolved in ACN/water = 50:50 (*v/v*) in the presence of 5 eq. 5'-GMP (at pH 7.4); Figure S61: HPLC chromatograms of **9** co-incubated with 5'-GMP and GSH; Figures S62 and S63: A2780wt/cis: Concentration-effect curves of **5**, **7**, **9–12**, cisplatin, and auranofin.

Author Contributions: Conceptualization, P.K. and H.P.V.; validation of biological assays, P.G.; X-ray measurements, K.W.; HPLC and DNA experiments, P.K.; *in vitro* testing, A.S.; writing—original draft preparation, P.K.; writing—review and editing, H.P.V., R.G. and B.K.; supervision, H.P.V. All authors have read and agreed to the published version of the manuscript.

Funding: P.K. is grateful to the Tiroler Wissenschaftsförderung (TWF) for the financial support (grant number: F.45021/8-2022).

Data Availability Statement: Not applicable.

Acknowledgments: We would like to thank Stefan Schwaiger and Michael Zwerger for technical support. The authors also like to thank Peter Enoh for measuring the ESI-HRMS spectra.

Conflicts of Interest: The authors declare no conflict of interest.

References

1. Rosenberg, B.; VanCamp, L.; Trosko, J.E.; Mansour, V.H. Platinum Compounds: A New Class of Potent Antitumour Agents. *Nature* **1969**, *222*, 385–386. [[CrossRef](#)]
2. Muggia, F.M.; Bonetti, A.; Hoeschele, J.D.; Rozenzweig, M.; Howell, S.B. Platinum Antitumor Complexes: 50 Years Since Barnett Rosenberg's Discovery. *J. Clin. Oncol.* **2015**, *33*, 4219–4226. [[CrossRef](#)]
3. Armstrong-Gordon, E.; Gnjudic, D.; McLachlan, A.J.; Hosseini, B.; Grant, A.; Beale, P.J.; Wheate, N.J. Patterns of Platinum Drug Use in an Acute Care Setting: A Retrospective Study. *J. Cancer Res. Clin. Oncol.* **2018**, *144*, 1561–1568. [[CrossRef](#)]
4. Desoize, B.; Madoulet, C. Particular Aspects of Platinum Compounds Used at Present in Cancer Treatment. *Crit. Rev. Oncol./Hematol.* **2002**, *42*, 317–325. [[CrossRef](#)]
5. Shah, N.; Dizon, D.S. New-Generation Platinum Agents for Solid Tumors. *Futur. Oncol.* **2009**, *5*, 33–42. [[CrossRef](#)]
6. Günes, D.A.; Florea, A.-M.; Spletstoesser, F.; Büsselberg, D. Co-Application of Arsenic Trioxide (As_2O_3) and Cisplatin (CDDP) on Human SY-5Y Neuroblastoma Cells has Differential Effects on the Intracellular Calcium Concentration ($[\text{Ca}^{2+}]$) and Cytotoxicity. *Neurotoxicology* **2009**, *30*, 194–202. [[CrossRef](#)]
7. Florea, A.M.; Büsselberg, D. Metals and Metal Compounds: Occurrence, Use, Benefits and Toxic Cellular Effects. *Biometals* **2006**, *19*, 419–427. [[CrossRef](#)]
8. Tsang, R.Y.; Al-Fayea, T.; Au, H.-J. Cisplatin Overdose. *Drug Saf.* **2009**, *32*, 1109–1122. [[CrossRef](#)]

9. Oun, R.; Moussa, Y.E.; Wheate, N.J. The Side Effects of Platinum-Based Chemotherapy Drugs: A Review for Chemists. *Dalton Trans.* **2018**, *47*, 6645–6653. [[CrossRef](#)]
10. Kelland, L. The Resurgence of Platinum-Based Cancer Chemotherapy. *Nat. Rev. Cancer* **2007**, *7*, 573–584. [[CrossRef](#)]
11. Ndagi, U.; Mhlongo, N.; Soliman, M.E. Metal Complexes in Cancer Therapy—An Update from Drug Design Perspective. *Drug Des. Devel. Ther.* **2017**, *11*, 599–616. [[CrossRef](#)]
12. Frezza, M.; Hindo, S.; Chen, D.; Davenport, A.; Schmitt, S.; Tomco, D.; Dou, Q.P. Novel Metals and Metal Complexes as Platforms for Cancer Therapy. *Curr. Pharm. Des.* **2010**, *16*, 1813–1825. [[CrossRef](#)]
13. Li, Y.; Liu, B.; Shi, H.; Wang, Y.; Sun, Q.; Zhang, Q. Metal Complexes Against Breast Cancer Stem Cells. *Dalton Trans.* **2021**, *50*, 14498–14512. [[CrossRef](#)]
14. Thota, S.; Rodrigues, D.A.; Crans, D.C.; Barreiro, E.J. Ru(II) Compounds: Next-Generation Anticancer Metallotherapeutics? *J. Med. Chem.* **2018**, *61*, 5805–5821. [[CrossRef](#)]
15. Höfer, D.; Varbanov, H.P.; Legin, A.; Jakupec, M.A.; Roller, A.; Galanski, M.S.; Keppler, B.K. Tetracarboxylatoplatinum(IV) Complexes Featuring Monodentate Leaving Groups—A Rational Approach Toward Exploiting the Platinum(IV) Prodrug Strategy. *J. Inorg. Biochem.* **2015**, *153*, 259–271. [[CrossRef](#)]
16. Lu, X.; Ma, X.; Chang, X.; Liang, Z.; Lv, L.; Shan, M.; Lu, Q.; Wen, Z.; Gust, R.; Liu, W. Recent Development of Gold(I) and Gold(III) Complexes as Therapeutic Agents for Cancer Diseases. *Chem. Soc. Rev.* **2022**, *51*, 5518–5556. [[CrossRef](#)]
17. Harringer, S.; Hejl, M.; Enyedy, É.A.; Jakupec, M.A.; Galanski, M.S.; Keppler, B.K.; Dyson, P.J.; Varbanov, H.P. Multifunctional Pt(IV) Prodrug Candidates Featuring the Carboplatin Core and Deferoxamine. *Dalton Trans.* **2021**, *50*, 8167–8178. [[CrossRef](#)]
18. Arduengo, A.J., III; Harlow, R.L.; Kline, M. A Stable Crystalline Carbene. *J. Am. Chem. Soc.* **1991**, *113*, 361–363. [[CrossRef](#)]
19. Jacobsen, H.; Correa, A.; Poater, A.; Costabile, C.; Cavallo, L. Understanding the M(NHC) (NHC=N-Heterocyclic Carbene) Bond. *Coord. Chem. Rev.* **2009**, *253*, 687–703. [[CrossRef](#)]
20. Díez-González, S. *N-heterocyclic Carbenes: From Laboratory to Curiosities to Efficient Synthetic Tools*; Royal Society of Chemistry: London, UK, 2016; Volume 27.
21. Bellemin-Lapponnaz, S. N-Heterocyclic Carbene Platinum Complexes: A Big Step Forward for Effective Antitumor Compounds. *Eur. J. Inorg. Chem.* **2020**, *2020*, 10–20. [[CrossRef](#)]
22. Cisnetti, F.; Gautier, A. Metal/N-Heterocyclic Carbene Complexes: Opportunities for the Development of Anticancer Metallo-drugs. *Angew. Chem. Int. Ed.* **2013**, *52*, 11976–11978. [[CrossRef](#)] [[PubMed](#)]
23. Böhme, M.D.; Eder, T.; Röthel, M.B.; Dutschke, P.D.; Wilm, L.F.B.; Hahn, F.E.; Dielmann, F. Synthesis of N-Heterocyclic Carbenes and Their Complexes by Chloronium Ion Abstraction from 2-Chloroazolium Salts Using Electron-Rich Phosphines. *Angew. Chem. Int. Ed.* **2022**, *61*, e202202190. [[CrossRef](#)] [[PubMed](#)]
24. Scattolin, T.; Nolan, S.P. Synthetic Routes to Late Transition Metal–NHC Complexes. *Trends Chem.* **2020**, *2*, 721–736. [[CrossRef](#)]
25. Zhao, Q.; Meng, G.; Nolan, S.P.; Szostak, M. N-Heterocyclic Carbene Complexes in C–H Activation Reactions. *Chem. Rev.* **2020**, *120*, 1981–2048. [[CrossRef](#)] [[PubMed](#)]
26. Yang, S.; Zhou, T.; Yu, X.; Szostak, M. Ag–NHC Complexes in the π -Activation of Alkynes. *Molecules* **2023**, *28*, 950. [[CrossRef](#)]
27. Shen, H.; Tian, G.; Xu, Z.; Wang, L.; Wu, Q.; Zhang, Y.; Teo, B.K.; Zheng, N. N-Heterocyclic Carbene Coordinated Metal Nanoparticles and Nanoclusters. *Coord. Chem. Rev.* **2022**, *458*, 214425. [[CrossRef](#)]
28. Liu, T.; Bai, S.; Zhang, L.; Hahn, F.E.; Han, Y.-F. N-Heterocyclic Carbene-Stabilized Metal Nanoparticles within Porous Organic Cages for Catalytic Application. *Natl. Sci. Rev.* **2022**, *9*, nwac067. [[CrossRef](#)]
29. Oehninger, L.; Rubbiani, R.; Ott, I. N-Heterocyclic Carbene Metal Complexes in Medicinal Chemistry. *Dalton Trans.* **2013**, *42*, 3269–3284. [[CrossRef](#)]
30. Büssing, R.; Karge, B.; Lippmann, P.; Jones, P.G.; Brönstrup, M.; Ott, I. Gold(I) and Gold(III) N-Heterocyclic Carbene Complexes as Antibacterial Agents and Inhibitors of Bacterial Thioredoxin Reductase. *ChemMedChem* **2021**, *16*, 3402–3409. [[CrossRef](#)]
31. Kaur, M.; Thakare, R.; Bhattacharya, A.; Murugan, P.A.; Kaul, G.; Shukla, M.; Singh, A.K.; Matheshwaran, S.; Chopra, S.; Bera, J.K. Antimicrobial Efficacy of a Hemilabile Pt(II)–NHC Compound Against Drug-Resistant *S. Aureus* and *Enterococcus*. *Dalton Trans.* **2023**, *52*, 1876–1884. [[CrossRef](#)]
32. Muenzner, J.K.; Rehm, T.; Biersack, B.; Casini, A.; de Graaf, I.A.M.; Worawutputtpong, P.; Noor, A.; Kempe, R.; Brabec, V.; Kasparkova, J.; et al. Adjusting the DNA Interaction and Anticancer Activity of Pt(II) N-Heterocyclic Carbene Complexes by Steric Shielding of the Trans Leaving Group. *J. Med. Chem.* **2015**, *58*, 6283–6292. [[CrossRef](#)] [[PubMed](#)]
33. Bouché, M.; Bonnefont, A.; Achard, T.; Bellemin-Lapponnaz, S. Exploring Diversity in Platinum(IV) N-Heterocyclic Carbene Complexes: Synthesis, Characterization, Reactivity and Biological Evaluation. *Dalton Trans.* **2018**, *47*, 11491–11502. [[CrossRef](#)]
34. Babu, T.; Ghareeb, H.; Basu, U.; Schueffl, H.; Theiner, S.; Heffeter, P.; Koellensperger, G.; Metanis, N.; Gandin, V.; Ott, I.; et al. Oral Anticancer Heterobimetallic Pt(IV)–Au(I) Complexes Show High In Vivo Activity and Low Toxicity. *Angew. Chem. Int. Ed.* **2023**, *62*, e202217233. [[CrossRef](#)] [[PubMed](#)]
35. Rehm, T.; Rothmund, M.; Muenzner, J.K.; Noor, A.; Kempe, R.; Schobert, R. Novel Cis-[(NHC)1(NHC)2(L)Cl]Platinum(II) Complexes—Synthesis, Structures, and Anticancer Activities. *Dalton Trans.* **2016**, *45*, 15390–15398. [[CrossRef](#)] [[PubMed](#)]
36. Rothmund, M.; Bär, S.I.; Rehm, T.; Kostrhunova, H.; Brabec, V.; Schobert, R. Antitumoral Effects of Mitochondria-Targeting Neutral and Cationic Cis-[Bis(1,3-Dibenzylimidazol-2-ylidene)Cl(L)]Pt(II) Complexes. *Dalton Trans.* **2020**, *49*, 8901–8910. [[CrossRef](#)]

37. Yang, Z.; Huang, S.; Liu, Y.; Chang, X.; Liang, Y.; Li, X.; Xu, Z.; Wang, S.; Lu, Y.; Liu, Y.; et al. Biotin-Targeted Au(I) Radiosensitizer for Cancer Synergistic Therapy by Intervening with Redox Homeostasis and Inducing Ferroptosis. *J. Med. Chem.* **2022**, *65*, 8401–8415. [[CrossRef](#)]
38. Rubbiani, R.; Can, S.; Kitanovic, I.; Alborzina, H.; Stefanopoulou, M.; Kokoschka, M.; Mönchgesang, S.; Sheldrick, W.S.; Wöfl, S.; Ott, I. Comparative in Vitro Evaluation of N-Heterocyclic Carbene Gold(I) Complexes of the Benzimidazolylidene Type. *J. Med. Chem.* **2011**, *54*, 8646–8657. [[CrossRef](#)]
39. Goetzfried, S.; Kapitzka, P.; Gallati, C.M.; Nindl, A.; Cziferszky, M.; Hermann, M.; Wurst, K.; Kircher, B.; Gust, R. Investigations on Reactivity, Stability and Biological Activity of Halido (NHC)gold(I) Complexes. *Dalton Trans.* **2022**, *51*, 1395–1406. [[CrossRef](#)]
40. Gallati, C.M.; Goetzfried, S.K.; Ausserer, M.; Sagasser, J.; Plangger, M.; Wurst, K.; Hermann, M.; Baecker, D.; Kircher, B.; Gust, R. Synthesis, Characterization and Biological Activity of Bromido[3-ethyl-4-aryl-5-(2-methoxy-pyridin-5-yl)-1-propyl-1,3-dihydro-2H-imidazol-2-ylidene]Gold(I) Complexes. *Dalton Trans.* **2020**, *49*, 5471–5481. [[CrossRef](#)]
41. Liu, W.; Bendorf, K.; Proetto, M.; Abram, U.; Hagenbach, A.; Gust, R. NHC Gold Halide Complexes Derived from 4,5-Diarylimidazoles: Synthesis, Structural Analysis, and Pharmacological Investigations as Potential Antitumor Agents. *J. Med. Chem.* **2011**, *54*, 8605–8615. [[CrossRef](#)]
42. Rubbiani, R.; Kitanovic, I.; Alborzina, H.; Can, S.; Kitanovic, A.; Onambele, L.A.; Stefanopoulou, M.; Geldmacher, Y.; Sheldrick, W.S.; Wolber, G.; et al. Benzimidazol-2-ylidene Gold(I) Complexes Are Thioredoxin Reductase Inhibitors with Multiple Antitumor Properties. *J. Med. Chem.* **2010**, *53*, 8608–8618. [[CrossRef](#)] [[PubMed](#)]
43. Goetzfried, S.K.; Koenig, S.M.C.; Gallati, C.M.; Gust, R. Internal and External Influences on Stability and Ligand Exchange Reactions in Bromido[3-ethyl-4-aryl-5-(2-methoxy-pyridin-5-yl)-1-propyl-1,3-dihydro-2H-imidazol-2-ylidene]gold(I) Complexes. *Inorg. Chem.* **2021**, *60*, 8546–8553. [[CrossRef](#)] [[PubMed](#)]
44. Goetzfried, S.K.; Gallati, C.M.; Cziferszky, M.; Talmazan, R.A.; Wurst, K.; Liedl, K.R.; Podewitz, M.; Gust, R. N-Heterocyclic Carbene Gold(I) Complexes: Mechanism of the Ligand Scrambling Reaction and Their Oxidation to Gold(III) in Aqueous Solutions. *Inorg. Chem.* **2020**, *59*, 15312–15323. [[CrossRef](#)]
45. Kapitzka, P.; Scherfler, A.; Salcher, S.; Sopper, S.; Cziferszky, M.; Wurst, K.; Gust, R. Reaction Behavior of [1,3-diethyl-4,5-diphenyl-2H-imidazol-2-ylidene] Containing Gold(I/III) Complexes Against Ingredients of the Cell Culture Medium and the Meaning on the Potential Use for Cancer Eradication Therapy. *J. Med. Chem.* **2023**, *66*, 8238–8250. [[CrossRef](#)]
46. Bertrand, B.; Stefan, L.; Pirrotta, M.; Monchaud, D.; Bodio, E.; Richard, P.; Le Gendre, P.; Warmerdam, E.; de Jager, M.H.; Groothuis, G.M.; et al. Caffeine-Based Gold(I) N-Heterocyclic Carbenes as Possible Anticancer Agents: Synthesis and Biological Properties. *Inorg. Chem.* **2014**, *53*, 2296–2303. [[CrossRef](#)]
47. Karaca, Ö.; Scalcon, V.; Meier-Menches, S.M.; Bonsignore, R.; Brouwer, J.M.J.L.; Tonolo, F.; Folda, A.; Rigobello, M.P.; Kühn, F.E.; Casini, A. Characterization of Hydrophilic Gold(I) N-Heterocyclic Carbene (NHC) Complexes as Potent TrxR Inhibitors Using Biochemical and Mass Spectrometric Approaches. *Inorg. Chem.* **2017**, *56*, 14237–14250. [[CrossRef](#)]
48. Unger, Y.; Zeller, A.; Taige, M.A.; Strassner, T. Near-UV Phosphorescent Emitters: N-Heterocyclic Platinum(II) Tetracarbene Complexes. *Dalton Trans.* **2009**, *24*, 4786–4794. [[CrossRef](#)]
49. Newman, C.P.; Deeth, R.J.; Clarkson, G.J.; Rourke, J.P. Synthesis of Mixed NHC/L Platinum(II) Complexes: Restricted Rotation of the NHC Group. *Organometallics* **2007**, *26*, 6225–6233. [[CrossRef](#)]
50. Rehm, T.; Rothmund, M.; Bär, A.; Dietel, T.; Kempe, R.; Kostrhunova, H.; Brabec, V.; Kasparkova, J.; Schobert, R. N,N-Dialkylbenzimidazol-2-ylidene Platinum Complexes—Effects of Alkyl Residues and Ancillary Cis-Ligands on Anticancer Activity. *Dalton Trans.* **2018**, *47*, 17367–17381. [[CrossRef](#)]
51. Wang, H.M.J.; Chen, C.Y.L.; Lin, I.J.B. Synthesis, Structure, and Spectroscopic Properties of Gold(I)–Carbene Complexes. *Organometallics* **1999**, *18*, 1216–1223. [[CrossRef](#)]
52. Rehm, T.; Rothmund, M.; Dietel, T.; Kempe, R.; Schobert, R. Synthesis, Structures and Cytotoxic Effects in Vitro of Cis- and Trans-[Pt(IV)Cl₄(NHC)₂] Complexes and Their Pt(II) Precursors. *Dalton Trans.* **2019**, *48*, 16358–16365. [[CrossRef](#)]
53. Wang, H.M.J.; Vasam, C.S.; Tsai, T.Y.R.; Chen, S.-H.; Chang, A.H.H.; Lin, I.J.B. Gold(I) N-Heterocyclic Carbene and Carbazolate Complexes. *Organometallics* **2005**, *24*, 486–493. [[CrossRef](#)]
54. Huynh, H.V.; Guo, S.; Wu, W. Detailed Structural, Spectroscopic, and Electrochemical Trends of Halido Mono- and Bis(NHC) Complexes of Au(I) and Au(III). *Organometallics* **2013**, *32*, 4591–4600. [[CrossRef](#)]
55. Kerrison, S.J.S.; Sadler, P.J. Solvolysis of Cis-[Pt(NH₃)₂Cl₂] in Dimethyl Sulphoxide and Reactions of Glycine with [PtCl₃(Me₂SO)][−] as Probed by ¹⁹⁵Pt Nuclear Magnetic Resonance Shifts and ¹⁹⁵Pt–¹⁵N Coupling Constants. *J. Chem. Soc. Chem. Commun.* **1977**, *23*, 861–863. [[CrossRef](#)]
56. Kerrison, S.J.S.; Sadler, P.J. ¹⁹⁵Pt NMR Studies of Platinum(II) Dimethylsulphoxide Complexes. *Inorganica Chim. Acta* **1985**, *104*, 197–201. [[CrossRef](#)]
57. Annibale, G.; Cattalini, L.; Canovese, L.; Michelon, G.; Marangoni, G.; Tobe, M.L. Reactivity of Sulfoxides Toward the Tetrachloroplatinate (II) Anion. *Inorg. Chem.* **1983**, *22*, 975–978. [[CrossRef](#)]
58. Hall, M.D.; Telma, K.A.; Chang, K.-E.; Lee, T.D.; Madigan, J.P.; Lloyd, J.R.; Goldlust, I.S.; Hoeschele, J.D.; Gottesman, M.M. Say no to DMSO: Dimethylsulfoxide Inactivates Cisplatin, Carboplatin, and Other Platinum Complexes. *Cancer Res.* **2014**, *74*, 3913–3922. [[CrossRef](#)]
59. Varbanov, H.P.; Ortiz, D.; Höfer, D.; Menin, L.; Galanski, M.S.; Keppler, B.K.; Dyson, P.J. Oxaliplatin Reacts with DMSO Only in the Presence of Water. *Dalton Trans.* **2017**, *46*, 8929–8932. [[CrossRef](#)]

60. Chen, H.H.; Kuo, M.T. Role of Glutathione in the Regulation of Cisplatin Resistance in Cancer Chemotherapy. *Met. Based Drugs* **2010**, *2010*, 430939. [[CrossRef](#)]
61. Schmidt, C.; Karge, B.; Misgeld, R.; Prokop, A.; Brönstrup, M.; Ott, I. Biscarbene Gold(I) Complexes: Structure–Activity–Relationships Regarding Antibacterial Effects, Cytotoxicity, TrxR Inhibition and Cellular Bioavailability. *MedChemComm* **2017**, *8*, 1681–1689. [[CrossRef](#)]
62. Messori, L.; Marchetti, L.; Massai, L.; Scaletti, F.; Guerri, A.; Landini, I.; Nobili, S.; Perrone, G.; Mini, E.; Leoni, P.; et al. Chemistry and Biology of Two Novel Gold(I) Carbene Complexes as Prospective Anticancer Agents. *Inorg. Chem.* **2014**, *53*, 2396–2403. [[CrossRef](#)] [[PubMed](#)]
63. Baik, M.H.; Friesner, R.A.; Lippard, S.J. Theoretical Study of Cisplatin Binding to Purine Bases: Why Does Cisplatin Prefer Guanine Over Adenine? *J. Am. Chem. Soc.* **2003**, *125*, 14082–14092. [[CrossRef](#)]
64. Lempers, E.L.M.; Reedijk, J. Interactions of Platinum Amine Compounds with Sulfur-Containing Biomolecules and DNA Fragments. *Adv. Inorg. Chem.* **1991**, *37*, 175–217.
65. Takahara, P.M.; Rosenzweig, A.C.; Frederick, C.A.; Lippard, S.J. Crystal Structure of Double-Stranded DNA Containing the Major Adduct of the Anticancer Drug Cisplatin. *Nature* **1995**, *377*, 649–652. [[CrossRef](#)]
66. Liu, Y.R.; Ji, C.; Zhang, H.Y.; Dou, S.X.; Xie, P.; Wang, W.C.; Wang, P.Y. Transplatin Enhances Effect of Cisplatin on Both Single DNA Molecules and Live Tumor Cells. *Arch. Biochem. Biophys.* **2013**, *536*, 12–24. [[CrossRef](#)] [[PubMed](#)]
67. Zhang, B.; Seki, S.; Akiyama, K.; Tsutsui, K.; Li, T.; Nagao, K. Detection and Analyses by Gel Electrophoresis of Cisplatin-Mediated DNA Damage. *Acta Med. Okayama* **1992**, *46*, 427–434. [[CrossRef](#)] [[PubMed](#)]
68. Chandra, A.; Pius, C.; Nabeel, M.; Nair, M.; Vishwanatha, J.K.; Ahmad, S.; Basha, R. Ovarian Cancer: Current Status and Strategies for Improving Therapeutic Outcomes. *Cancer Med.* **2019**, *8*, 7018–7031. [[CrossRef](#)]
69. Lopez, J.; Banerjee, S.; Kaye, S.B. New Developments in the Treatment of Ovarian Cancer-Future Perspectives. *Ann. Oncol.* **2013**, *24* (Suppl. S10), x69–x76. [[CrossRef](#)]
70. Abdalbari, F.H.; Telleria, C.M. The Gold Complex Auranofin: New Perspectives for Cancer Therapy. *Discov. Oncol.* **2021**, *12*, 42. [[CrossRef](#)]
71. Gamberi, T.; Chiappetta, G.; Fiaschi, T.; Modesti, A.; Sorbi, F.; Magherini, F. Upgrade of an Old Drug: Auranofin in Innovative Cancer Therapies to Overcome Drug Resistance and to Increase Drug Effectiveness. *Med. Res. Rev.* **2022**, *42*, 1111–1146. [[CrossRef](#)]
72. Alatise, K.L.; Gardner, S.; Alexander-Bryant, A. Mechanisms of Drug Resistance in Ovarian Cancer and Associated Gene Targets. *Cancers* **2022**, *14*, 6246. [[CrossRef](#)] [[PubMed](#)]
73. Borkar, P.; Bhandari, P.; Yadav, S.; Prabhu, A. Cisplatin Resistance in Ovarian Cancer: Classical Outlook and Newer Perspectives. *Biomed. Pharmacol. J.* **2021**, *14*, 1993–2005. [[CrossRef](#)]
74. Liu, W.; Bendsdorf, K.; Proetto, M.; Hagenbach, A.; Abram, U.; Gust, R. Synthesis, Characterization, and in Vitro Studies of Bis[1,3-diethyl-4,5-diarylimidazol-2-ylidene]gold(I/III) Complexes. *J. Med. Chem.* **2012**, *55*, 3713–3724. [[CrossRef](#)]
75. Gallati, C.M.; Goetzfried, S.K.; Ortmeier, A.; Sagasser, J.; Wurst, K.; Hermann, M.; Baecker, D.; Kircher, B.; Gust, R. Synthesis, Characterization and Biological Activity of Bis[3-ethyl-4-aryl-5-(2-methoxy-pyridin-5-yl)-1-propyl-1,3-dihydro-2H-imidazol-2-ylidene]Gold(I) Complexes. *Dalton Trans.* **2021**, *50*, 4270–4279. [[CrossRef](#)]
76. Price, J.H.; Williamson, A.N.; Schramm, R.F.; Wayland, B.B. Palladium(II) and Platinum(II) Alkyl Sulfoxide Complexes. Examples of Sulfur-Bonded, Mixed Sulfur- and Oxygen-Bonded, and Totally Oxygen-Bonded Complexes. *Inorg. Chem.* **1972**, *11*, 1280–1284. [[CrossRef](#)]
77. Sheldrick, G.M. SHELXT—Integrated Space-Group and Crystal-Structure Determination. *Acta Crystallogr. Sect. A Found. Adv.* **2015**, *71*, 3–8. [[CrossRef](#)] [[PubMed](#)]
78. Sheldrick, G.M. Crystal Structure Refinement with SHELXL. *Acta Crystallogr. Sect. C Struct. Chem.* **2015**, *71*, 3–8. [[CrossRef](#)]

Disclaimer/Publisher’s Note: The statements, opinions and data contained in all publications are solely those of the individual author(s) and contributor(s) and not of MDPI and/or the editor(s). MDPI and/or the editor(s) disclaim responsibility for any injury to people or property resulting from any ideas, methods, instructions or products referred to in the content.